A Geophysical Investigation of Hydraulic Pathways at the Panola Mountain Research Watershed

A Thesis
Presented to
The Academic Faculty

by

Gabriel Hebert

In Partial Fulfillment
Of the Requirements for the Degree
Master of Science in Geophysics

Georgia Institute of Technology
December 2005

A Geophysical Investigation of Hydraulic Pathways at the Panola Mountain Research Watershed

Approved by:

Dr. Leland Timothy Long, Chair
School of Earth and Atmospheric Sciences
Georgia Institute of Technology

Dr. Robert Lowell
School of Earth and Atmospheric Sciences
Georgia Institute of Technology

Dr. Daniel Lizarralde
School of Earth and Atmospheric Sciences
Georgia Institute of Technology

Date Approved: 8/25/05

ACKNOWLEDGEMENTS

I would like to thank my advisor, Dr. Tim Long, for introducing me to the topic of shallow earth geophysics. Without his endless patience and help, this work would not have been possible. I would also like to express my appreciation to Dr. Dan Lizarralde and Dr. Robert Lowell for their additional support and service on my thesis committee, as well as Jake Peters of the U.S.G.S, and Ilja Tromp-van Meerveld for their cooperation and help. I would like to express my gratitude to my fellow students in arms: Tatiana Toteva, Sawyer Gosnell, Yang Yang, and Shelly Tyre. Finally, I would like to thank my wife for her constant support in my academic endeavors, my family for their agape love and encouragement, and my God for creating me with a passion for learning about the physical world.

TABLE OF CONTENTS

LIST OF TABLES

LIST OF FIGURES

SUMMARY

The Panola Mountain Research Watershed (PMRW) is a 41 ha (16.6 km^2) forested watershed, located 25 km southeast of Atlanta, Georgia. Within that watershed is a 10 ha (4.05 km^2) sub-catchment, which contains the headwaters of the watershed's main stream as well as two outcrops of Panola Granite (granodiorite composition) (Burns et al. 2001). On the hill-slope below the northernmost outcrop, is a 20m long trench that has been excavated down to bedrock, a depth that ranges from 0.5-1.5m. In previous studies (Burns et al., 2001; Freer, et al., 2002), discharge through the overlying soils was measured along the trench in 2m sections across the full length of the trench, by tipping-bucket gages. In those studies, it was assumed that the underlying bedrock was impermeable. However, Burns et al. (2003) used Chlorofluorocarbon and tritium/helium-3 dating techniques to show that the riparian groundwater downslope from the trenched hillslope site was only 6 to 7 years old, thus casting doubt on the previous assumption. The permeability of the Panola granite in question was proven by a recent Lithium-Bromide line tracer experiment that was performed 11 m above the trench Tromp-van Meerveld et al., in review). Due to the levels of bromide in the bedrock measured at the trench, it has become apparent that fluid is being lost to hidden hydraulic pathways, those probably being fractures.

The objective of this thesis is to test the viability of using shallow seismic reflection (SSR) to map out fracture zones at the trenched hillslope site, using GPR and shallow seismic refraction as supplemental techniques to verify the interpretation. In this study, data from two seismic common shot point (CSP) surveys permitted an image of

the soil/bedrock interface to be constructed, as well as enabling an acoustic velocity profile to be calculated for the study area. This velocity profile is then used with data from five reflection surveys (one seismic and four radar) to create vertical profiles of the shallow subsurface. Although the resulting SSR profile is less than optimum, the maximum coherent energy is only 2 times greater than the noise, higher amplitude arrivals related to structure were still able to be detected. From this profile, as well as those from the GPR survey, it can be concluded that the proposed hidden hydraulic pathways do indeed exist, and also that they can be accurately (0.2-0.4 m accuracy) mapped out using GPR and SSR survey methods.

Chapter 1

Introduction

1.1 Overview

The hydrology of the Panola Mountain Research Watershed (PMRW) has been well studied over the past 10 years (Freer et al., 1997; Freer et al., 2002; Peters et al., 2003). A complete list of publications has been maintained by the U. S. Geological Survey, Atlanta, Ga. office (please see http://ga.water.usgs.gov/projects/**panola**/ga103biblio.html). One particular area that has been studied in depth is the hillslope below the northernmost rock outcrop. There, a 20m long trench has been excavated down to bedrock. In previous studies (Burns et al., 2001; Freer, et al., 2002), discharge through the overlying soils was measured along the trench in 2m sections across the full length of the trench by tipping-bucket gages. In those studies, it was assumed that the underlying unweathered Panola Granite was virtually impermeable. The basis for this assumption is that the measured hydraulic conductivity of Panola granite cores was $7*10^{-6}$ m/yr (White et al., 2001). However, recent studies have shown that assumption to be incorrect. Burns et al. (2003) used Chlorofluorocarbon and tritium/helium-3 dating techniques to show that the riparian groundwater down slope from the trenched hillslope site was only 6 to 7 years old, thus casting doubt on the previous assumption. The permeability of the underlying bedrock was determined during a 2002 Lithium- Bromide line tracer experiment (Figure1.1) that was performed 11 m above the trench, across the entire length (Tromp-van Meerveld et al., in review).

Because of the high levels of bromide in the bedrock at the trench, Tromp-van Meerveld et al. (in review) deduced that fluid is being lost to hydraulic pathways in the bedrock. A map of fracture location and intensity below the soil layer could help to fully understand the hydrology of the PMRW, particularly the trenched hillslope site. However to date, no studies have been done to image or locate these pathways.

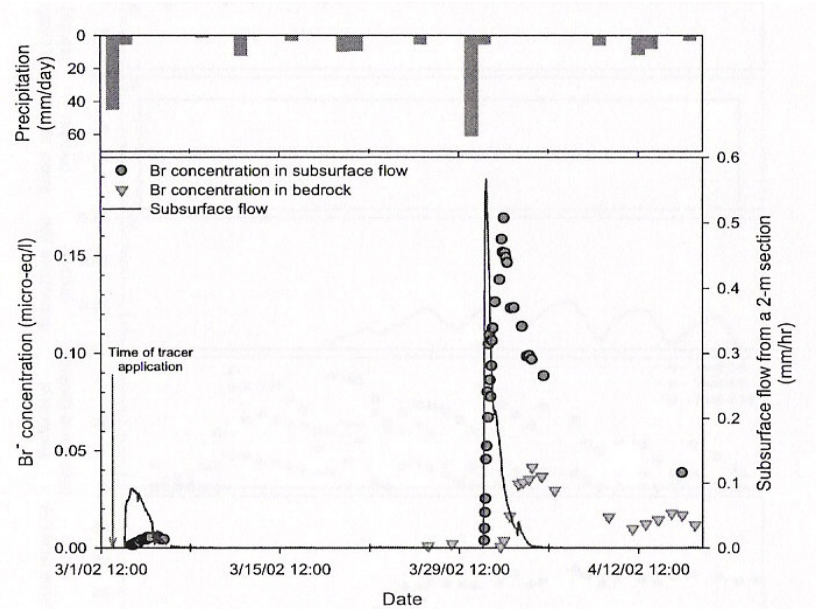

Figure 1.1 The Lithium-Bromide line tracer experiment. The bromide in the bedrock is measured at the trench after the storm event on 3/29/02. The sustained concentrations of Lithium-Bromide were interpreted by Tromp-van Meerveld et al. (in review) to show that significant fluids were moving through the bedrock.

In the study of shallow engineering and geophysical applications, there is a lack of controlled, nondestructive, high resolution mapping tools for mapping fracture zones (Ghose et al., 1998). While the high resolution of GPR has made it a popular, noninvasive tool for shallow studies, it has depth limitations. A common limitation occurs in soft, conductive soils, where GPR has a maximum penetration depth of only

2-3 m (Ghose et al., 1998). In cases like this, or where other geophysical techniques, such as conventional seismic reflection/refraction or electrical methods, offer too poor a resolution, a different tool is needed. The objective of this thesis is to test the viability of using shallow seismic reflection (SSR) to map out fracture zones at the trenched hillslope site. Ground penetrating radar and shallow seismic refraction will be used as supplemental techniques to verify the interpretation of the SSR data.

1.2 Site Characterization

The Panola Mountain Research Watershed (PMRW) is a 41 ha ($4.1*10^5$ m^2) forested watershed, which is located 25 km southeast of Atlanta, Georgia (Figure 1.2). The PMRW is located in the Georgia Piedmont, a region characterized by highly folded and deformed mid to high grade metamorphic rocks such as schists and gneisses. The Piedmont also contains intrusions of various granitic units, like the Panola Mountain granite and Lithonia Gneiss, in the vicinity of PMRW. Panola Mountain may be considered a remnant of differential erosion, because the granites resist erosion much better than the amphibolite gneiss and other rock units with a higher content of feldspars. Elevation in the watershed ranges from 222 m in the valley to 279 m on top of the outcrops (Freer, 2002). The soils consist mostly of sandy loams, Inceptisols of the Ashlar series Entisols of the Wake series, and Ultisols of the Gwinnett and Pacolet series; which are colluvial on the hill-slopes and alluvial in the valley (Zumbuhl, 1998). The soils, which are overlain by a ≈ 0.15 m mangle of humus, are generally 0.5 m to 1.5 m thick and overlie saprolite, whose thickness ranges from 0 m on some of the hill-slope to 10 m in the valley (Freer et al., 2002; Burns et al., 2003; Tromp-van Meerveld, in review).

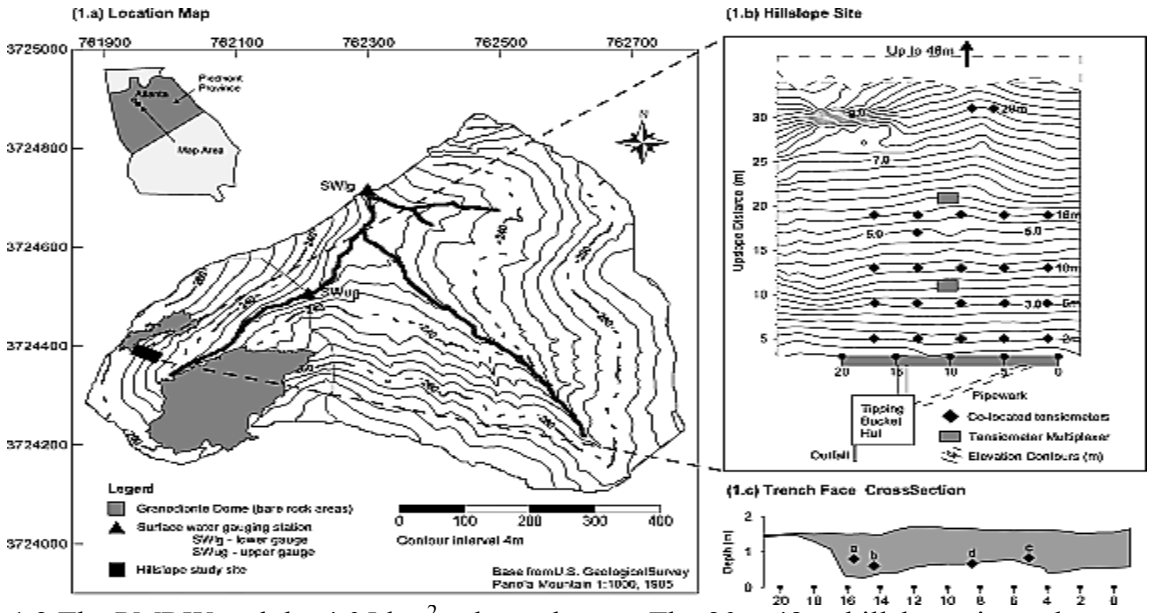

Figure 1.2 The PMRW and the 4.05 km^2 sub-catchment. The 20 × 48 m hillslope site and a cross-section of the trench have been enlarged. (from Freer et al., 2002)

The southwest corner of the watershed (Figure 1.2) is a 10 ha ($1.0*10^5$ m^2) sub-catchment contained entirely within the PMRS. This sub-catchment contains the headwaters of the watershed's mainstream, as well as two outcrops of Panola Granite. The Panola Granite, which is described by Burns et al. (2001) and White et al. (2002) as a biotite-muscovite-oligoclase-quartz-mircrocline granodiorite, was intruded into the Clairmont Formation approximately 290-360 MY ago.

On the hillslope below the northernmost outcrop is a 20m long trench that has been excavated down to bedrock (Figure 1.2). This portion of the hillslope was the chosen for this study for two reasons. First, it was chosen because numerous other studies (Burns et al., 2003; Freer et al., 2002; Tromp-van Meerveld et al., in review; Zumbuhl, 1998) have been conducted at this location, and consequently there is extensive

information describing this study area. Second, as mentioned by Burns et al. (2003), there is no saprolite in this study area above the trench. The lack of saprolite simplifies the study by allowing for a two-layer model. The high velocity contrast between the overburden and rock should provide reflections to be observed from the bedrock, as well as allowing the fractures zones to be imaged.

1.3 Techniques Used

The purpose of this thesis was to study the viability of using shallow seismic reflection (SSR) to map out fracture zones at the trenched hill-slope site within the PMRW. Although the principal technique used was SSR, three supplemental techniques were used as well to help assess its viability: ground penetrating radar (GPR), shallow seismic refraction, and two knocking pole surveys. This section discusses the fore mentioned techniques, beginning with SSR and ending with the knocking pole surveys.

1.3.1 Shallow Seismic Reflection (SSR)

Faults, fracture zones, and other hydraulic pathways have been mapped and studied using seismic reflection for many years, but typically these studies were reserved for deeper targets. This was partly due to the cost and size of instruments, the non-uniformity of near-surface materials, and partly because of the economic incentive for using reflection seismology to located deep structures in the search for oil (Pakiser and Mabey, 1954). In 1954, L.C. Pakiser and D. R. Mabey of the United States Geological Survey, were the first to publish an example of finding a seismic reflector shallower than 50 m (Steeples, 1998). Due to the high cost of surveys, the application of seismic

techniques to shallow or near-surface targets was mostly abandoned, until it reemerged in the 1970's and 1980's. Since then, seismic equipment and techniques have vastly improved, as well as becoming more cost efficient. Recently, an interest in techniques to study the near surface has grown, with increased attention to environmental hazards and pollution in near-surface soils. However, despite this renewed interest, the seismic reflection methods have had limited utilization in the shallow near-surface soils. Among the reasons for this, are the high attenuation properties of the soils, the significant heterogeneity of the near surface, and competing simpler techniques such as ground penetrating radar (GPR) or direct sampling techniques. None-the-less, a few attempts at shallow reflection interpretation have been performed at the University of Kansas Geology Department. In recent studies (Baker et al., 2001; Baker et al., 1999; Steeples and Miller, 1998) reflectors have been imaged as shallow as 1-2 m with vertical resolutions of 0.1-0.15 m, thus approaching the current resolution of ground penetrating radar (GPR) for similar depths. It should be noted though, that these studies are the exception.

The shallow seismic reflection survey for this study was conducted using an in-house seismic recording system. This system consists of a 16 bit-A/D converter with 16 channels that was connected to a field laptop computer. The detectors for this survey consisted of 16, 100 Hz geophones. The seismic data were recorded at a sampling frequency of 6.25 kHz and a record length of 640 ms.

1.3.2 Ground Penetrating Radar (GPR)

GPR was first developed in the late 1950's to study ice thicknesses and permafrost, but it wasn't until the 1970's and 1980's that it became a popular tool for obtaining high resolution images of the shallow subsurface, largely due once again to the tremendous progress in technology (Conyers, 1997; Cook, 1995). Currently, high frequency antennas can obtain sub-centimeter resolution, but with a greatly reduced depth of penetration. Due to its potential for high resolution imaging, as well as the ease of surveying, GPR has been used in numerous applications: determining thicknesses of stratagraphic layers, detecting underground voids, mapping contamination plumes, and even measuring fluid saturation in soils (Parasnis, 1997). The application that makes it valuable to this study is its ability to detect faults and fractures (Demanet et al., 2001; Rashed and Nakagawa, 2004; Stevens et al., 1995; Toshioka et al., 1995). However, because GPR is often limited in its penetration depth, it is frequently used with other geophysical methods, commonly other electrical methods or seismic methods. In this study, GPR is used to validate the seismic methods, in an attempt to assess the capabilities of seismic reflection to map out hydraulic pathways at the Panola Mountain Research Watershed (PMRW).

Within the last ten years, GPR has begun to be used in conjunction with shallow seismic methods to study the shallow subsurface. Baker et al. (2001) used GPR to map out three stratagraphic layers within the upper two meters. Cardimona et al. (1998) used GPR and SSR to image a shallow aquifer. Most important to this study though, is the recent use of these two geophysical methods to map out faults and fractures. Chow et al. (2001), Rashed and Nakagawa (2004), Demanet et al. (2001), and Bano et al. (2002), have successfully used GPR and seismic reflection to study dip-slip faults. Similarly,

Derobert and Abraham (2000) used the two methods to locate fractures in a gypsum quarry.

GPR and shallow seismic methods compliment each other for several reasons. The first reason is their differences in depth penetration. Because GPR is normally limited to imaging the upper 10 m of the earth, seismic reflection and refraction can be used to image the desired structure at greater depth (Baker et al., 2001). The second reason these two can be incorporated with such success, is the similarity of the two techniques. A GPR survey is essentially the electromagnetic equivalent of a standard seismic reflection survey (Cook, 1995). Hence, similar processing techniques and codes can be used to process both sets of data. Another benefit to using GPR and SSR together is an increased understanding of the physical properties of the subsurface (Baker, 2001). Reflections seen by seismic surveys arise from differences in acoustic impedance (which is directly related to density and the elastic parameters) between different media, so seismic reflections are more sensitive to the rock matrix (Liu, 1997) than radar waves. In contrast, reflections seen in radar surveys are due to differences in the electromagnetic properties of the media, such as the dielectric permittivity, magnetic permeability, and electrical conductivity (Baker et al., 2001).

The ground penetrating radar used for this study was a Mala Ramac system. The reflection surveys were conducted with a shielded 250 MHz towable antenna and the corresponding survey wheel. The transmitter-receiver spacing within the antenna housing was 0.36m and the trace interval was held constant at 10 cm. The sampling frequency for this antenna was 2574 MHz, giving 360 samples per trace. Each final trace consisted of two stacked measurements.

1.3.3 Shallow Seismic Refraction

Of the two seismic techniques used in this study, seismic refraction is the oldest. By 1912, Gutenberg had used refraction techniques to discover the earth's core, as well as to calculate its depth (Dobrin, 1976). In the 1920's, the seismic refraction technique was used to locate salt domes, and in turn, oil (Musgrave, 1967). Of the two techniques, it is also the more widely used, being more economically efficient than reflection seismology (Dobrin, 1976). Typically, it is used as a preliminary method, to determine the velocity structure of the subsurface, as well as mapping different refracting layers.

The seismic refraction survey conducted for this study used a Geometrix SmartSeis S12 seismograph. This seismograph consisted of an A-T compatible computer with an 80386SX microprocessor, a printer, a 16 bit-A/D converter, and a display screen. The geophones used consisted of 12, 40 Hz Geometrix geophones. The seismic records taken were 96 ms in length and had a sampling frequency of 16.1 kHz.

1.3.4 Knocking Pole Surveys

A knocking pole survey consists of pounding a metal rod into the ground until refusal. Because it is has been determined from previous studies (Burns et al., 2003) that there is no saprolite in this area, then the distance the rod travels in the soil is the measured depth to bedrock, or possibly an isolated unweathered rock above bedrock. Two knocking pole surveys were used in this study to validate the depth to bedrock. Zumbuhl (1998) performed a knocking pole survey with a spacing of two meters on the

hill slope upslope from the trench (Figures 1.3-1.6, Table 1.1) to determine the depth to bedrock.

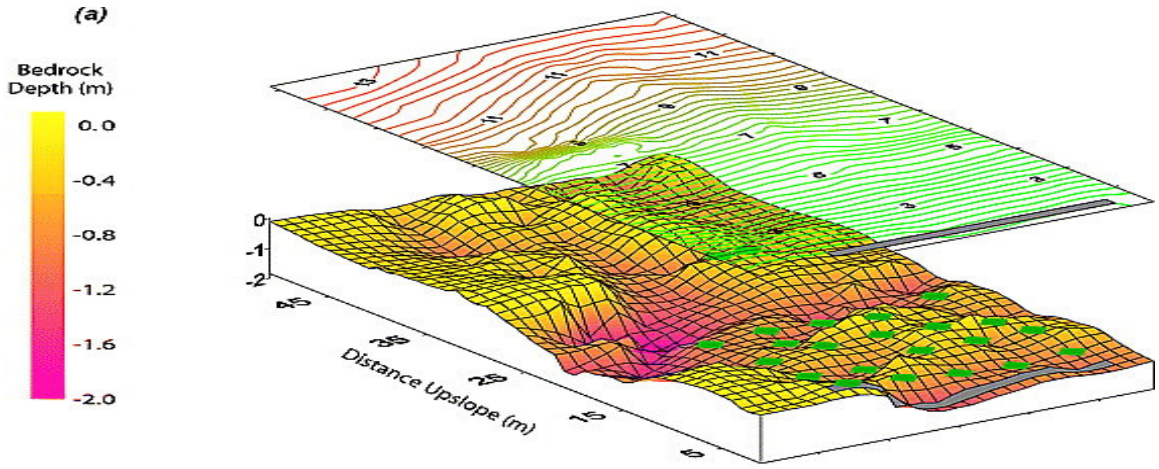

Figure 1.3 A compilation depth to bedrock image of the study site. This figure was produced by the DTA performed on the data from the 1998 Zumbuhl knocking pole survey. The trench is represented by the grey line (from Zumbuhl, 1998).

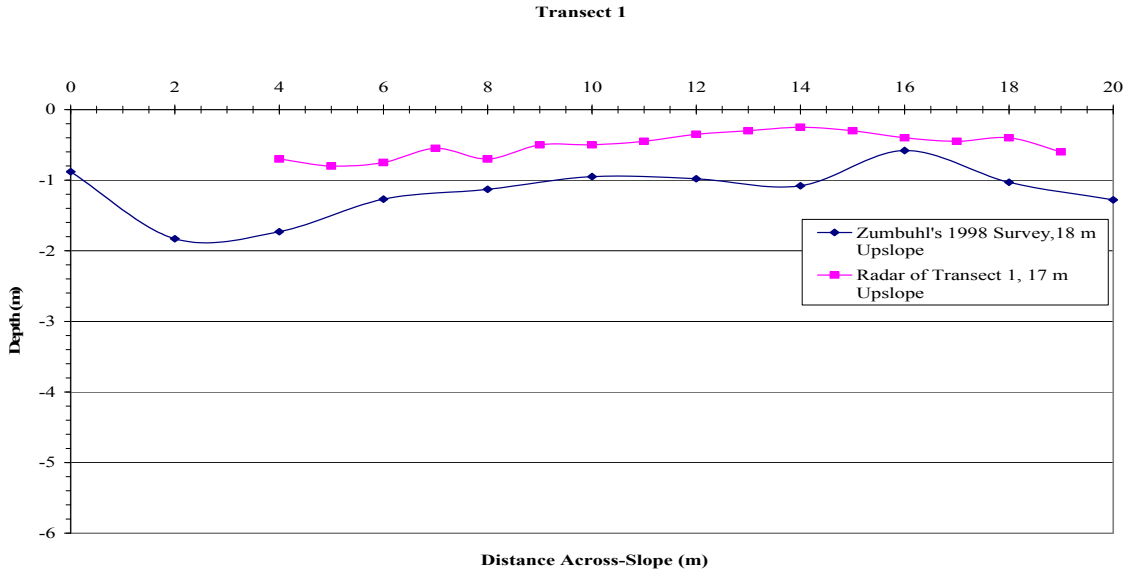

Figure 1.4 Depth to bedrock along Transect 1. The actual Transect 1 is 17 m upslope from the trench. The results of Zumbuhl's knocking pole survey 18 m upslope are given as a reference.

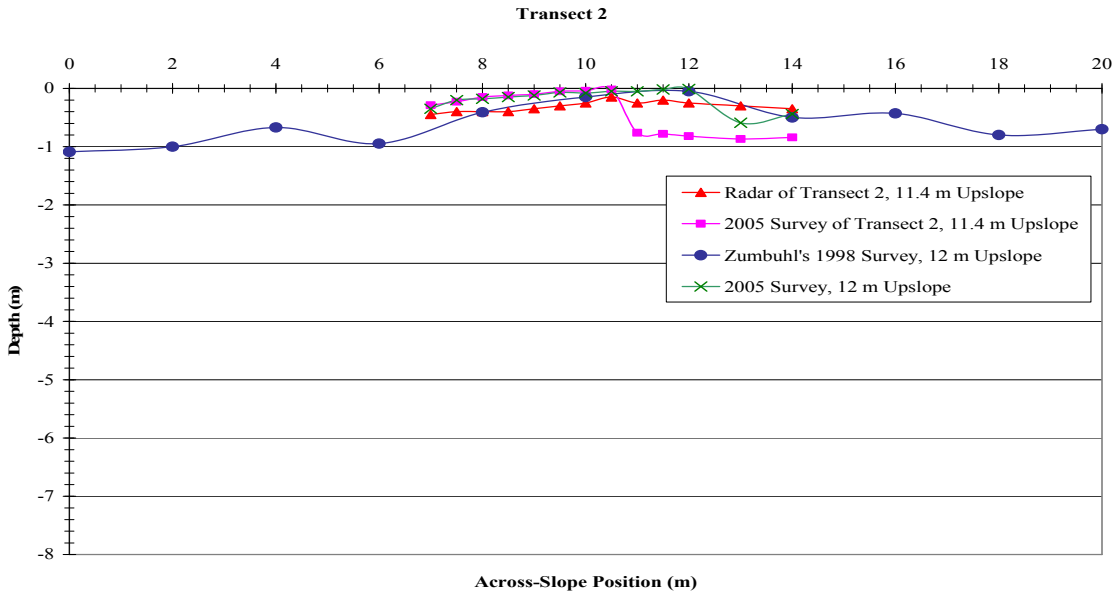

Figure 1.5 Depth to bedrock along Transect 2. The squares and triangles are the knocking pole results. The actual Transect 2 was 11.4 m upslope. The 12 m values are compared to Zumbuhl's 12 m values.

Figure 1.6 Depth to bedrock along Transect 3. The radar and seismic data were taken along Transect 3, which was 3 m upslope, whereas the Zumbuhl (1998) survey was 4 m upslope. Notice that the radar closely follows the 2005 survey, except that the depths are deeper.

Table 1.1: Zumbuhl's 1998 Knocking Pole Survey. The knocking pole survey conducted by Zumbuhl (1998). Note: the 0 m upslope is the trench wall. Also, for consistency with this study, the notation of the original data was altered, so the 0 m across slope points were labeled as 20 m in Zumbuhl's study. The actual locations are the same.

	X -Value (Across Slope) (m)										
Y-Value (Upslope) (m)	0	2	4	6	8	10	12	14	16	18	20
0	0.08	0.05	0.43	1.22	1.32	1.05	0.96	0.86	0.84	1.1	0.97
2	0.1	0.45	0.49	0.5	0.7	0.75	0.97	0.99	1	0.89	0.82
4	0.58	0.69	0.89	0.81	0.24	0.55	0.62	0.6	0.8	0.69	0.41
6	0.2	0.62	0.85	1	0.9	0.74	0.41	0.47	0.89	0.62	0.57
8	0.54	0.77	0.62	0.58	0.68	0.68	0.28	0.2	0.08	0.32	0.5
10	1.17	0.89	0.66	0.56	0.63	0.57	0.47	0.49	0.55	0.63	1.21
12	1.09	1	0.67	0.95	0.41	0.15	0.05	0.5	0.43	0.8	0.7
14	1.23	0.98	0.9	0.89	1.26	0.89	0.33	0.3	0.61	0.77	0.62
16	1.37	0.99	0.96	0.82	0.86	0.92	1	1.29	0.99	1	0.51
18	1.72	1.2	1.06	0.9	0.78	0.91	1.39	0.93	1.4	1.02	0.95
20	0.88	1.83	1.73	1.27	1.13	0.95	0.98	1.08	0.58	1.03	1.28
22	1.86	1.81	1.48	1.23	0.97	0.86	0.61	0.69	0.83	0.46	0.44
24	1.48	0.82	1.48	1.27	1.08	0.76	0.53	0.32	0.46	0.58	0.7
26	0	0	0.84	1.11	1.12	0.69	0.39	0.5	0.32	0.4	0.46
28	0	0.03	0.55	1.02	0.95	0.4	0.33	0.32	0.55	0.34	0.34
30	0.22	0.34	0.46	0.81	0.86	1.04	0.73	0.2	0.48	0.33	0.36
32	0.39	0.81	0.08	0.84	1.07	0.63	0.17	0.13	0.46	0.6	0.5
34	0.24	0.45	0.4	0.67	0.87	0.29	0.05	0.17	0.4	0.68	0.58
36	0.6	0.24	0.48	0.58	0.77	0.41	0.01	0.11	0.53	0.68	0.69
38	0.57	0.65	1.07	0.65	0.78	0.49	0.18	0.27	0.7	0.59	0.57
40	0.79	1.06	0.62	0.46	0.44	0.31	0.01	0.27	0.67	0.67	0.74
42	0.76	0.9	0.43	0.46	0.77	0.31	0	0.05	0.7	0.77	0.75
44	0.53	0.77	0.26	0.03	0	0.5	0.54	0.82	0.83	0.64	0.25
46	0.21	0.75	0.41	0	0.43	0.77	0.22	0.86	0.48	1.2	0.25

Table 1.2: Knocking Pole Survey Conducted for This Study. Here are the depths found in the knocking pole survey conducted for this study.

Profile 2			Profile 3		
Line Position	Depth		Line Position	Depth	
	11.4 m Upslope	12 m Upslope		3 m Upslope	4 m Upslope
7	-0.29	-0.35	5	-0.6	-0.79
7.5	-0.23	-0.2	6	-0.56	-0.74
8	-0.15	-0.18	7	-0.64	-0.8
8.5	-0.12	-0.15	8	-0.4	-0.56
9	-0.1	-0.12	9	-0.49	
9.5	-0.05	-0.07	10	-0.67	-0.57
10	-0.04	-0.08	11	-0.72	
10.5	-0.02	-0.05	12	-0.75	-0.68
11	-0.76	-0.05	14	-0.71	-0.71
11.5	-0.78	-0.02	16	-1.18	-0.96
12	-0.82	-0.01			
13	-0.87	-0.59			
14	-0.84	-0.44			
15	-0.86	-0.48			

A knocking pole survey (Figures 1.5 and 1.6, Table 1.2) was performed along Transects 2 and 3 during this study, for two reasons. First, the transects chosen for this study were between points in the Zumbuhl study. Second, the soil deposition and erosion could have measurably changed the thickness of overburden. However, the differences between the two were subtle, the mean being only 11 cm. These two surveys were used as ground truth for bedrock depths throughout this study.

The terrain that made up the study site had an average gradient of 25°. For this reason, transect locations were chosen for areas that had minimal topographic changes along the length of the profile, and areas that had minimal tree and underbrush

obstructions (Figure 1.7). The following section will go into detail about the governing theory of the three primary techniques used, and well as discuss the actual process used.

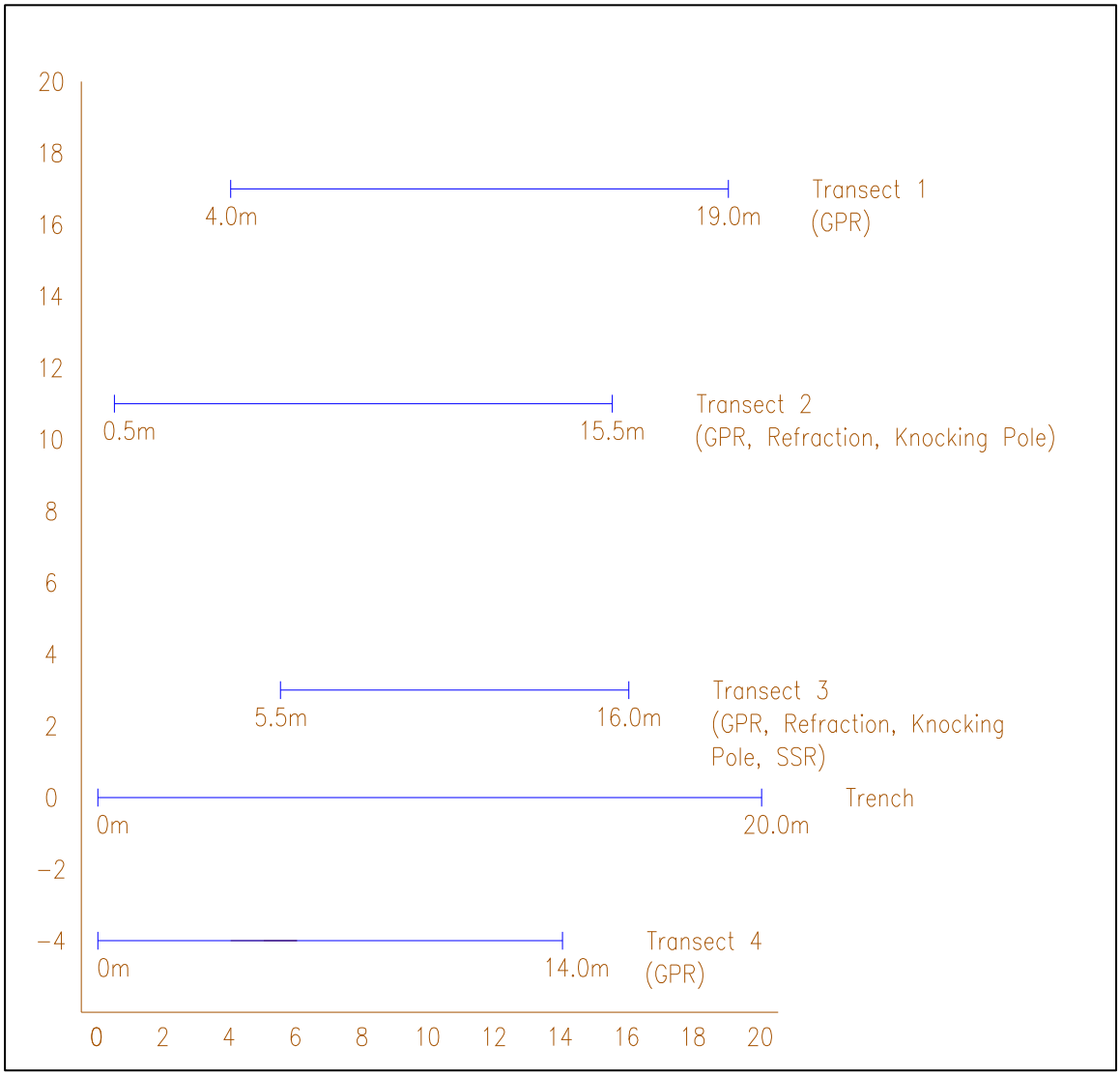

Figure 1.7 Diagram of the study site. The types of surveys performed at each transect are listed.

Chapter 2

Theory and Procedure

2.1 Theory

This section presents the theory of the three primary methods used in this study, beginning with SSR, following then by GPR, and ending with shallow seismic refraction. The next section will discuss the procedure of the surveys conducted for each technique.

2.1.1 Shallow Seismic Reflection (SSR)

In the seismic reflection technique, seismic waves are generated at the surface, usually by an impulsive source. The seismic waves travel through an elastic medium until they come to a portion of the media with a contrast in acoustic impedance (Z). The acoustic impedance is the product of the density (ρ) and the seismic velocity. Part of the wave that strikes the change in acoustic impedance is reflected or scattered. Those waves scattered back to the surface can be detected by an array of receivers called geophones. Seismic waves exist as body waves and surface waves. The body waves of interest in most reflection surveys are the higher frequency P-waves. The surface waves generated by a surface source are dominated by lower frequencies and hence the surface waves are usually removed by low-cut filtering. The necessity of the filtering process will be discussed at the end of this section.

The equations of motion for a homogeneous, isotropic, elastic medium predict the existence of two wave equations: one for a P-waves and one for an S-waves. The wave equation for a P-wave potential, Φ, which is similar to the EM wave equation, is given by Equation 2.1

$$\nabla^2\Phi - (1/\alpha^2)\partial^2\Phi/\partial t^2 = 0 \tag{2.1}$$

where α is the P-wave velocity. The wave equation governs the movement of the wave through an elastic material. The P-wave velocity of waves in an elastic material is dependent on the density and the elastic properties of that material. It is given as

$$\alpha = \sqrt{\lambda + 2\mu/\rho} \tag{2.2}$$

where λ is known as Lame's constant, μ is the sheer modulus, and ρ is the density (Lay and Wallace, 1995).

When a wave hits the interface between two media, it can do one of three things: reflect, refract, or diffract. The analysis of seismic travel times for a wave is facilitated by using the high frequency approximation. The wave ray is the direction of propagation of a wave and its direction is governed by Snell's Law (Parasnis, 1997). Snell's law is written as follows:

$$\sin\theta_i/\ v_1 = \sin\theta_{rl}/\ v_1 = \sin\theta_{rf}/\ v_2 \tag{2.3}$$

where θ_i is the angle of incidence, θ_{rl} is the angle of reflection, θ_{rf} is the angle of refraction, v_1 is the velocity of the wave in medium 1, and v_2 is the velocity of the wave in medium 2 (Figure 2.1). For a perfectly planar surface, $\theta_i = \theta_{rl.}$ In this section, only the reflected and diffracted waves will be discussed.

When the acoustic wave comes to a boundary that has a difference in acoustic impedance, part of the wave can be reflected back towards the surface. The amount of energy reflected, is dependant on the difference in acoustic impedance between the two media, as is shown in Equation 2.4

$$R = (Z_2 - Z_1)/(Z_2 + Z_1) \tag{2.4}$$

where R is the reflection coefficient of normal incidence, Z_1 is the acoustic impedance of medium 1, and Z_2 is the acoustic impedance of medium 2 (Gueguen and Palciauskas, 1994). This equation is very similar to that of the reflection coefficient in GPR surveys. Likewise, the reflection equations that relate travel time to depth and lateral position are the same for GPR surveys. The time for a wave to travel down and back from a reflecting layer can be written as

$$t = (t_o^2 + x^2 / v^2)^{1/2} = 2/v\{z^2 + (x/2)^2\}^{1/2} \tag{2.5}$$

where $t_o = 2z/v,$ is the direct travel time to the reflector and back (Parasnis, 1997).

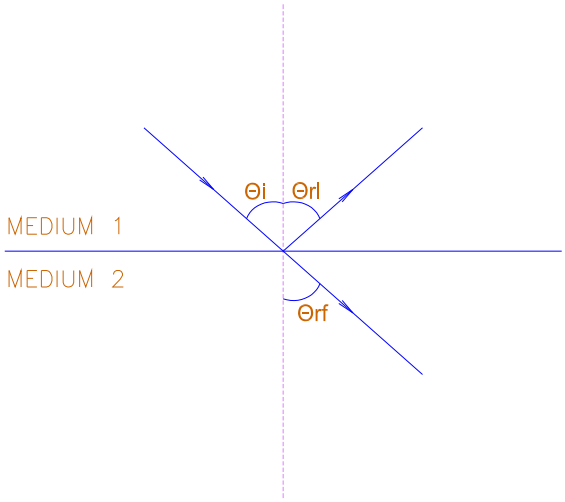

Figure 2.1 A visual of Snell's Law. Here the incident wave strikes the medium1 and medium2 interface, where part of the incident energy is reflected, and part is refracted. In this study, medium1 was soil and medium2 was bedrock.

Using Equation 2.5, one can then solve for the depth (z).

$$z = 1/2(v^2t^2 - x^2)^{1/2} \tag{2.6}$$

As the source-receiver offset is increased, the reflected arrival is delayed, and eventually with distance, it asymptotically approaches the direct arrival. This increase in arrival time with increased distance from the shot is called "move out." In seismic reflection processing, reflected waves can be enhanced by summing waves that have reflected from the same point. Generally, they are from shot points and geophone pairs that are at different separations. This is known as common mid point (CMP) stacking. Hence, in order to add coherent waves, the arrival times of the reflected waves from a flat surface need to be corrected for moveout. The moveout time correction (Δt) is $\Delta t = t\text{-}t_o$, which applied to Equation 2.5 is

$$\Delta t = (t_o^2 + x^2 / v^2)^{1/2} - t_o \tag{2.7}$$

where v here is the move-out velocity. The normal moveout (NMO) correction is applied by subtracting the NMO Δt from the travel time of the reflection, making it correspond to the vertical two-way time at a point half way between the source and the detector. The main difficulty in this correction lies in choosing the correct move-out velocity. If there are enough points on the reflection hyperbola, then t^2 can be plotted against x^2, the slope of which is $1/v^2$. If there still are not enough points, then by a process of trial and error, the velocity is obtained that gives the best result. This process works for reflectors that have small dips and are almost horizontal. However, for a steeply dipping reflector or a point reflector, a migration routine must be run to obtain the correct image.

While the primary objectives in a reflection survey are the reflected waves, the diffracted waves must be addressed as well. Waves are diffracted at discontinuities in the medium that are smaller than the wavelength of the wave that intersects them. The travel time of a wave diffracted off of a small inhomogeneity (or the edge of a reflector) is

$$t_d = (z/v) + (x^2 + z^2)^{1/2}/v \tag{2.8}$$

where the first term is the travel time down to the point of diffraction, and the second term is the travel time from that point to the detector (Parasnis, 1997). Thus, to correct for diffraction moveout, the direct travel time ($t_o = 2z/v,$) would be subtracted from Equation 2.8.

While the design of the data acquisition is the same for SSR surveys as deeper ones, the importance of certain aspects of the physics differs significantly between the two (Steeples, 1998). Although much smaller offset must be used to obtain the necessary resolution desired in shallow surveys, they are not simply a scale down from deeper crustal studies. For example, high frequency sources and geophones are critical to shallow surveys because shallow small reflectors require much higher dominant frequencies (usually several hundred Hz) than deeper reflectors in order to resolve layers. While the higher frequencies needed to resolve thin shallow layers makes shallow reflections easy to filter out from the lower frequency surface waves, it also makes them difficult to distinguish between direct and refracted waves. This is not a problem with reflections from deeper interfaces, whose lower frequencies can be easily contaminated by the surface waves (Steeples and Miller, 1998). Another problem that occurs in shallow surveys alone is due to the airwaves. Most seismic sources generate air-blast noise, be it from explosions or simply a falling sledgehammer. When this noise couples to the ground, or to the geophones, it is called an airwave (Steeples and Miller, 1998). While this problem is not important in deeper studies, it can be quite daunting to a shallow study. Because airwaves usually have a dominant frequency above 100 Hz, filtering them can be a problem. Whenever these waves can be distinguished from other

waves, it is best to surgically mute them. All these issues, along with the high attenuation properties of the soils and the often-significant lateral heterogeneity of the near surface, make shallow seismic studies a difficult task.

2.1.2 Ground Penetrating Radar (GPR)

A GPR is a geophysical tool that transmits high frequency radio pulses (chirps) into the ground and measures the time between transmission and reception of pulses reflected back to the instrument (Conyers, 1997). If the velocity of the electromagnetic (EM) wave is known for the given media, it is possible to translate the travel times of reflected waves into the corresponding depths to the reflecting boundaries, thus giving an "image" of the subsurface. If the velocity is not known for the given media, it can be obtained by plotting travel time versus receiver offset and taking the inverse of the slope. These are the same principals that are used in seismic reflection and refraction studies, except the pulses used here are EM waves, whereas seismic pulses consist of acoustic waves.

Where seismic reflections are caused by changes in seismic velocities between two media, radar reflections are caused by discontinuities in the electrical properties (that is the conductivity and permittivity) of the medium in which the EM wave is traveling (Parasnis, 1997). These discontinuities are usually due to one of two things: changes in the concentration (or conductivity) of pore fluid or lithologic changes (Conyers, 1997). The electromagnetic field is very sensitive to the fluid contents in the pore space (Liu, 1997). An increase in the fluid content in a medium increases the conductivity, which in turn results in greater signal losses, and poorer depth penetration. Maxwell's equations

can be manipulated to give an equation for propagation of electromagnetic waves. The equation for an electric field in a dielectric medium is

$$\nabla^2 E = \sigma\mu_o \partial E/\partial t + \varepsilon\mu_o \partial^2 E/\partial t^2 \quad (2.9)$$

where E is the electric field, μ_o is the magnetic permeability of free space, σ is the conductivity, and ε is the electric permittivity of the material (Gueguen and Palciauskas, 1994). The conductivity (σ) and electric permittivity (ε) are responsible for radar reflections. The electric permittivity for a given medium can be written as

$$(\varepsilon = \varepsilon_0 K) \quad (2.10)$$

where ε_o is the permittivity of free space, and K is known as the dielectric constant. The dielectric constant controls the speed of an EM wave in a particular medium, as is shown in the following equation:

$$v = c/\sqrt{K} = c/n = \lambda f \quad (2.11)$$

where v is the velocity of the wave in the dielectric material, c is the speed of electromagnetic radiation in a vacuum (=2.998 x 10^8m/s), n is the index of refraction, which is simply equal to the square root of the dielectric constant, λ is the wavelength, and f is the frequency. As fore mentioned, the pore fluid plays a large role in the performance of a GPR, by affecting the conductivity of the medium. As the wave travels down through the ground, it is attenuated. In order to understand this better, it is necessary to split the dielectric constant (which can easily be switched out with the index of refraction) into a real and imaginary part:

$$K = K_r + iK_i \quad (2.12)$$

where r means real and i means imaginary. Once that is done, the ratio of K_i and K_r are taken to create a loss tangent:

$$\tan\delta = K_i / K_r = \sigma/\omega\varepsilon \tag{2.13}$$

where σ is the conductivity, ω is the angular frequency $(= 2\pi f)$, and ε is the electric permittivity. Using the loss tangent, the penetration depth L can be written as:

$$L = \lambda / 2\pi \tan\delta\sqrt{K_r} = \lambda\sqrt{K_r} / 2\pi K_i \tag{2.14}$$

Thus, one can see that the penetration depth of the GPR is a function of both wavelength (which is related to frequency), and the components of the dielectric constant (Elachi, 1987).

Once the radio wave is in the ground, it will eventually come to some reflecting material where a portion of the incident energy will be reflected back towards the surface. This reflected portion, also known as the reflection coefficient (R) or reflectivity, is related to the difference in dielectric constant between the two materials. For normal incidence by the following equation:

$$R = (\sqrt{K_1} - \sqrt{K_2}) / (\sqrt{K_1} + \sqrt{K_2}) \tag{2.15}$$

It is quite clear then, that the amount of energy reflected increases as the difference between dielectric constants increases (Conyers, 1997).

There are two types of GPR profiling, stationary or continuous. During stationary profiling, a transmitter and a receiver are offset by a set distance, the measurement is taken, and then everything is moved to the next station. Bi-static antennas are used in this type of survey. The second type is continuous profiling. This was the style used for this study. During this type of profiling, both antennas are in one housing, which is dragged along a transect. If u is the dragging speed, the spacing between scans is

$$s = uf_s\tau_w/f_r \quad (2.16)$$

where f_s is the sampling frequency, τ_w is the time window, and f_r is the repetition frequency (Parasnis, 1997). The scan spacing (also known as the trace spacing) for this study, was 10 cm. Once the radar profile has been obtained, the travel times to the reflectors need to be converted into depths. This can be done using Equations 2.5 and 2.6 from the seismic section. Another feature of radar profiles that is similar to seismic profiles, are the diffraction hyperbolas. These occur from inhomogeneities within the medium that are the same size or smaller than the dominant wavelength of the antenna being used. The hyperbolas can be reduced down to a single point, located at the apex by applying a migration routine.

2.1.3 Shallow Seismic Refraction

Seismic refraction is similar to seismic reflection in that it also uses elastic waves to map out the different stratagraphic layers in the subsurface. However, it is the mode of wave propagation that differentiates this technique from seismic reflection surveys. In reflection seismology, the geophysicist looks for waves that have been directly reflected from a contrasting medium, but in seismic refraction studies, one must look for the incoming waves that have traveled directly through the differing media (Figure 2.2). In this study the geologic scenario was a single layer of soil overlying Panola granite. Whereas in the reflection survey, the reflected waves bounced directly off of the soil/bedrock interface, the refracted waves travel down through the soil, through the

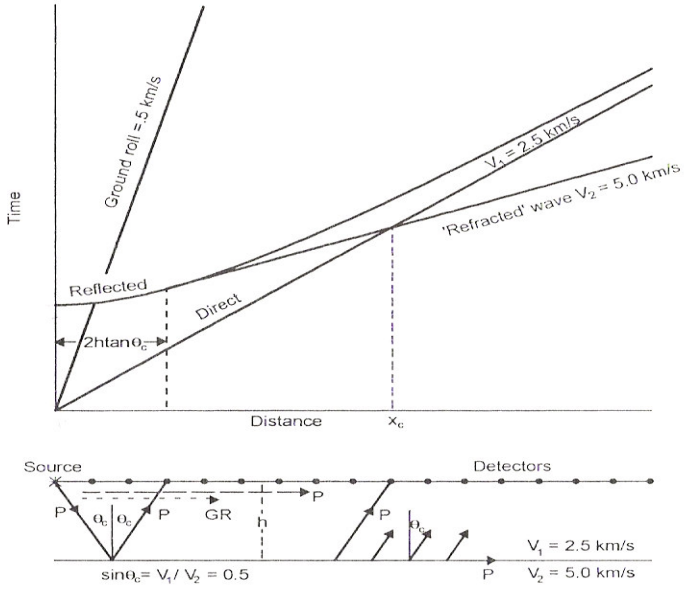

Figure 2.2 A typical time-distance graph. It is easily seen that once the offset reaches the critical point, the refracted wave arrives before the direct wave (from of Parasnis, 1997).

bedrock, and back up through the soil (Figure 2.2). Waves are reflected off and refracted through the interface until the angle of incidence reaches the critical angle (θ_c), after which, the incident waves are critically refracted through the higher velocity medium. At the critical angle of incidence, the angle of refraction (θ_{rf}) is equal to 90 degrees, if the velocity in medium 2 (v_2) is greater than the velocity in medium 1 (v_2). From Snell's Law (Equation 2.3), one can see how the critical angle is related to the velocities of the two layers.

$$\sin \theta_c / v_1 = \sin \theta_{rf} / v_2 = 1 / v_2 \rightarrow \theta_c = \sin^{-1}(v_1 / v_2) \qquad (2.16)$$

The travel time for the refracted wave is

$$t = (1/v_2)\, x + (2z_1 \cos \theta_c / v_1) \qquad (2.17)$$

where z_1 is the depth to medium 2 for a given lateral position (Parasnis, 1997). In Equation 2.17, that the slope for the line representing the refracted wave on a time-

distance graph (Figure 2.2) is $(1/v_2)$, and the intercept of that line with the x = 0 axis is the delay time, given by the second part. The intercept is known as the delay time (δt_1) for the upper layer, which is medium 1. The lateral position where the refracted waves arrive first is known as the crossover distance or break point (x_c). Now, x_c is the point on the time-distance graph where the travel time line for the direct wave and the refracted wave intersect, then by equating the direct wave with Equation 2. 17, it is apparent that

$$x_c = 2z_1[(v_2 - v_1)/(v_2 - v_1)]^{/12} \quad (2.18)$$

If the crossover point is clearly visible on the time-distance graph, and if the velocities for both of the media are known, then Equation 2.18 can be solved for z_1 at that point.

Another way of calculating the depth to bedrock is by using the Delay Time Method (Bohidar and Hermance, 2002; Dobrin, 1976). This method finds the delay time under a given receiver point, then uses that time to solve for the depth under that point. Figure 2.3 shows two shots in opposite directions (A and C), the refracted arrivals of both being seen by receiver B. From before, we know that the delay time is $\delta t_b = 2z_b \cos \theta_c / v_1$, but it can also be written as a function of travel times

$$\delta t_b = (t_{ab} + t_{cb} - t_{reciprocal})/2 \quad (2.19)$$

where t_{ab} is the travel time from shot A to receiver B, t_{cb} is the travel time from shot C to receiver B, and $t_{reciprocal}$ is the travel time from point A to point C, and vice versa. Then, once Δt_b has been determined, from its own definition, the depth under point B can be determined

$$\delta t_b = 2z_b \cos \theta_c / v_1 \rightarrow z_b = \delta t_b v_1 /2 \cos\theta_c \quad (2.20)$$

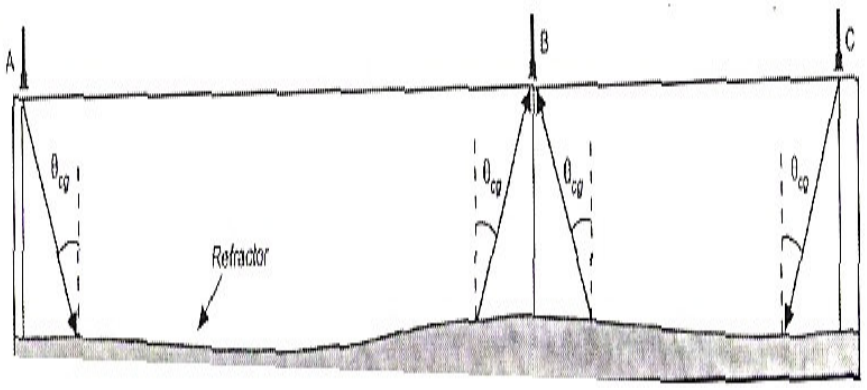

Figure 2.3 A visual of the Delay Time Method. It is used to determine depths down to a refractor (from Parasnis, 1997).

This technique is very useful for imaging a refractor, but it does have certain stipulations. First, it is assumed that the refractor is not necessarily horizontal, but locally planar beneath each receiver point. Second, it is assumed that distances measured at the surface are approximately the same as distances on the refractor, that is, small dip angles (less than 20°). Finally, this technique can only be used to calculate depths beneath receiver points that have actually received refracted waves from both shots. The refraction lines in this study were limited by the unexpected short length of reversed paths.

Another assumption made is that the refractor velocity (v_2) is constant over the length of the refractor. This is not always the case. Varying lithology, as well as fractured areas can affect the velocity. One method of determining the different velocities within a given refractor is the 'mean-minus-t' or MMT method (Parasnis, 1997). To better visualize how this method works, please see Figure 2.4. If t_a is the arrival time of a refracted wave at a receiver origination from one direction, and t_b is the arrival time at that same receiver, but from the opposite direction, then the difference between those two times is obviously $\Delta t = t_b - t_a$. It can then be shown that

$$\Delta t/2 = (t_b + t_a)/2 - t_a \qquad (2.21)$$

where the first term on the right is the mean arrival time, and the second term is the time itself. If $\Delta t/2$ is calculated for each receiver point that detects refracted waves from both shot directions, then those points can be plotted, preferably from any arbitrary reference time line. The points can then be connected by straight line segments, the inverse slope of which is the refractor velocity for that section. These velocities are important, as they play a large role in any refraction calculation.

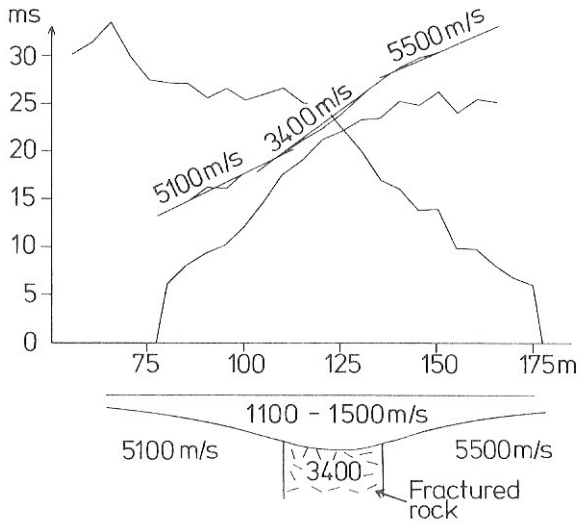

Figure 2.4 The MMT method is used to find refractor velocities. Notice that the refractor velocities can only be calculated for the points located in between the two break points (from Parasnis, 1997).

2.2 Procedure

Now that the general theories regarding shallow seismic reflection, ground penetrating radar, and seismic refraction have been presented, the methods and processing techniques applied in this study will be given. As in the section before, the

SSR study will be presented first, followed by the GPR study, and then finally the shallow seismic refraction study. All directions and distances given in the following procedures will use the reference point of 0 m (20 m in Figure 1.2) along the trench, facing upslope.

2.2.1 Shallow Seismic Reflection

Of the three methods applied in this analysis, SSR involved the greatest care in field acquisition techniques, as well as the most processing time. Although there has been an increased interest in this geophysical method within past ten years or so (Black et al., 1994; Baker et al., 1998; Baker et al., 1999; Ghose et al, 1998; Jefferson et al., 1998; Keiswetter and Steeples, 1995; Steeples et al., 1999), SSR still remains a difficult, time-consuming technique for shallow applications. This is due to the inherent difficulties in obtaining quality reflection data within the upper few meters, including: difficulties in generating and recording high frequency data; the heterogeneity of the near surface velocity structure; and the interference of surface, air, and shallow refracted waves with reflected arrivals. However, certain things can be done to make the process as efficient as possible. Many of these were implemented in this study. For example, Steeples et al. (1999) improved the portability of a linear geophone array by attaching the array to a board. This allows the array to be moved as a whole, as opposed to each geophone individually. In this study, 1.27 cm (1/2 in) holes were drilled into a standard pine 2.44 m (8 ft) by 5.08 cm (2 in) by 2.54 cm (1 in) every 5 cm along the length of the board. The geophones where then placed every 5 cm for the first part of the line and every 10 cm for the latter part.

Another means of improving the shallow seismic survey was in the source design and usage. Typical sources used in shallow seismic surveys include: explosives (Dobrin, 1976), projectiles (Steeples et al., 1999; Baker et al., 1999), portable vibrators (Ghose et al., 1998), and sledgehammers (Keiswetter and Steeples, 1994; Baker et al., 1997). Generally, the first three are preferred due to their ability to generate higher frequencies, which are critical in SSR surveys. However, because the PMRW is located in the Panola State Conservation Park, the use of explosives and projectiles was not allowed, and because a vibrator system was not available, a home-made modified sledgehammer source, known as a rotational impact device (RID) was used. The RID source used in this study is based on the design of Keiswetter and Steeples (1994). Essentially, a RID is a seismic source that uses gravity as a consistent mechanism for repeatable energy impacts (Keiswetter and Steeples, 1995). The RID used in this study was not as advanced as the one used by Keiswetter and Steeples because it was not attached to an all terrain vehicle for easy transport, but its performance was not compromised by the design change. The RID consisted of a 9.1 Kg (20 lb) sledgehammer with a 1 m handle, a 5 cm by 15 cm by 1m (2in by 6 in by 39 in) board, two sturdy L brackets, and a $9.5*10^{-3}$ m (3/8 in) bolt. To assemble the device, the two L brackets were bolted to the board. Then, a hole slightly larger than the bolt was drilled 0.9 m down the handle from the center of the hammer. The bolt, which acted like an axel, was then inserted through one L bracket, through the sledgehammer, and then through the other L bracket, before being fastened by a nut. The hammer could then be rotated to vertical and released. The hammer was attached such that the head would impact orthogonal to the ground. Thus, because the hammer was raised to the same height every shot, the impact energy should remain mostly constant.

Also, besides giving a repeatable source, this RID also greatly reduced the amount of energy expended by the surveyor per shot, thus allowing for more shots to be taken per survey.

According to Baker et al. (1997), optimizing the energy put into the ground is equally or more important to data quality than optimizing how the energy is collected coming out of the ground. For this reason, other measures were also taken in attempt to obtain better quality data. For example, Keiswetter and Steeples (1995) showed that larger hammer masses and plate areas increased the amount of seismic energy released in the ground by as much as 6 dB, as well as shifting the peak frequencies 40 Hz higher on average, without preferentially increasing the amount of surface waves generated. Because the use of explosive, projectile, or vibrator sources was not possible for this study, these suggestions were implemented in attempts to improve the results of the sledgehammer source. The hammer used had a mass of 9.1 kg (20 lb). A $6.4*10^{-3}$ m (1/4 in) thick steel plate, with a radius of 0.3 m (approx. 1ft), resulting in a surface area of 0.29 m^2, was used as the impact surface in this survey. To increase the portability of this plate, two U-bolts, one on each side, were fastened to the edges. Finally, Baker et al. (1997) showed that sledgehammer surveys performed on wet or damp soil, generate higher frequencies than when performed on dry soil, because the plate couples better to the soil. For this reason, the seismic survey was performed when the soil conditions were damp.

The shallow seismic reflection survey consisted of one transect taken 3 m upslope from the trench, using the acquisition system designed by Dr. Tim Long, sixteen 100 Hz geophones, the RID, and the plate described above. The survey consisted of 72 shots, all

with a common offset of 0.35 m, taken over 24 stations, that is, 3 shots per station. All shots were examined, with the best quality (minimal ringing, no double bounce of hammer) shot gather being used for that station. Typically, all three shots per station would be added, but the lack of consistency between shots permitted simple summation. In order to study the importance of geophone spacing and fold on the resolution, the survey was split into three parts. The first section consisted of stations 1-4, which were located from 0 to1.95m along the line. In this first section, the geophone spacing was 5 cm and the shot spacing was 0.4 m, giving single fold coverage. The second section consisted of stations 5-14, which were located from 1.60 to 3.25 m along the transect. Here, the geophone spacing was kept at 0.05 m, but the shot spacing was decreased to 0.1m, giving 4 fold coverage. The final section consisted of stations 15 – 24, which were located from 2.9 to 10.1m along the transect. For this section, the geophone spacing was increased to 0.1 m and the shot spacing was increased to 0.8 m, once again giving single fold coverage.

The seismic reflection data was processed using a temporary license of Visual SUNT, a program designed by the Rockware company out of Golden, Colorado. Visual SUNT is a windows-based version of Seismic Unix (SU), the seismic processing program designed by the Center for Wave Phenomenon at the Colorado School of Mines. The process applied to the SSR data was as follows. First, the files were converted from DAT files produced by the acquisition software into SU files. Second, the shooting geometry and some of the acquisition parameters were entered into the SU data files. Third, the 384 traces were appended into one large data file. Fourth, a band-pass filter was applied from 350 Hz to 1200 Hz in order to suppress the surface waves. Fifth, the amplitudes of the

traces were normalized using an AGC algorithm with a time window of 30 ms. Sixth, a deconvolution routine was run in attempt to identify and remove multiples from the seismic record. Seventh, the data were sorted by CDP number, and within the CDP, by offset. Once the record was sorted, a 0-75 ms window was run on the data to remove the record later than 75 ms. Because of the shallow depth being dealt with in this study, only the beginning part of the record was needed. Next, the first 10 ms of the record was muted to avoid stacking first arrivals. The next step in the process was to apply the normal-moveout (NMO) correction. However, before this could be done, the moveout velocity had to be determined for the major reflector, in this case, the soil/bedrock interface. Under normal circumstances, this would not pose a problem, but because the largest CDP gather only had 4 points, the moveout was not accurately defined. The analysis resorted to a process of trial and error, and from that process, it was determined that the best moveout velocities were 1000 m/s at 13 ms and 5000 m/s at 30 ms. Using those values, the NMO correction was applied, and the data was then stacked. After stacking the data, another band pass (600-1000) filter was applied and a predictive deconvolution routine was applied. Finally, all amplitudes less than 10% of the maximum amplitude were removed in order to emphasize the higher amplitude reflections.

2.2.2 GPR

The GPR system used in this study was a Mala Geoscience Ramac system, which included the CU2 control unit, the 250 MHz shielded antenna, measuring wheel, and corresponding monitor. The GPR survey performed at the trenched hillslope site

consisted of four, southwest to northeast transects, each parallel to the trench, with three being upslope, and one down-slope (Figure 1.7) from the trench. The locations of these transects along the hillslope were determined by finding lines with a clear line of sight. Once the system was all connected, the necessary parameters such as time window and sampling frequency were entered into the monitor, recording was started, and the antenna was dragged along the length of the transect. On completion of all four transects, the data were processed using a processing software developed by Mala Geosciences, called Rad Explorer. The processing routine was a standard one for typical GPR data. First, the DC offset was removed, deleting the constant component of the signal in the data. Next, an automatic gain control (AGC) routine was run, increasing amplification by equalizing the amplitudes within a time window which was best determined to be (30 ns), for each trace. This allowed some of the deeper reflections to be seen. Then, the background noise of the traces was cancelled by removing the average amplitude within a running window. At this point in the data reduction, the air/soil interface was clearly discernable, so the time was adjusted, setting the zero mark to the air/soil interface. Next, a band pass filter was applied, increasing the signal/noise ratio. Then, a Stolt F-K Migration routine was applied. This is the migration algorithm created by Stolt, used in the frequency (F) and wavenumber (K) domain. This algorithm reduces diffraction hyperbolas down to a single point. Finally, the velocities in the soil and bedrock were calculated by fitting diffraction hyperbolas in each medium. Once the velocities were determined, a depth model could be created by applying the previously determined velocities to the soil and bedrock layers seen on the GPR profile.

2.2.3 Shallow Seismic Refraction

The shallow seismic refraction consisted of two common shot point (CSP) surveys, one taken along Transect 2 and one taken along Transect 3. In both surveys, the Geometrix Smart Seis S12 was used, along with the corresponding twelve, 40 Hz geophones. The source used was the rotational impact device

The survey along Transect 2 consisted of 24 shots, 12 in each direction. The geophones were spaced every 0.1 m, giving an array length of 1.1 m. The geophone line was moved after each shot with a spacing of 1.2m, giving a geophone every 0.1 m along the total length of the transect. Shots 1 – 12 were conducted left to right, starting at 2 m and going to 16 m. The shot point was located at 1 m for each shot. Shots 13-24 were conducted right-to-left, starting at 16 m and going to 2 m. The shot point was located at 17 m for each shot.

Transect 3 consisted of 31 shots: 15 left-to-right (SW to NE) and 16 right-to-left (NE to SW). The left-to-right section consisted of two lines. The first line consisted of 9 shots, and went from 5.6 m to 16.3 m. The source offset was -1m, so the shot point was located at 4.6 m. The second line consisted of 6 shots, with geophones starting at 9.1 m and going to 16.2 m. The source offset was -0.5m, so the source was located at 8.6 m. The right-to-left section consisted of two lines as well. The first line consisted of 9 shots, starting at 16.3 m and going to 5.6 m. The source offset was +1 m, so the source point was at 17.3 m. The second line was made up of 7 shots, beginning at 16.2 m and going to 0.1 m. The source offset was +0.5 m, so the source as located at 16.7 m.

Once the data were taken and appended into one file, the geometry was entered and the data were filtered (100-650 Hz and 300-800 Hz). Then the first breaks were

picked and plotted versus offset. This allowed the velocities to be calculated. Finally, based on the measured velocities, the average and the maximum critical angles were determined using Equation 2.16, and the time delay method was applied (Equations 2.19 and 2.20), giving an image of the bedrock topography.

Chapter 3

Results

This study addressed the ability of seismic reflection to first, detect fractures at very shallow depths, and second, use the fractures and topography to identify the path of water down the slope. The resolution of the SSR is evaluated by a comparison with data from the other field techniques. Within each section, several issues will be discussed, including whether the geophysical method was able to image the hidden fracture zones in the bedrock, whether the resolution of the survey was sufficient, and whether the profiles compare favorably to what is known from the ground truth.

3.1 Shallow Seismic Reflection (SSR)

The SSR survey was processed as a profile. The profile indicated some of the structures suggested by the supplemental techniques. However, significant attention to details in data acquisition was required to obtain usable results. Care is needed in laying out geophones, to make sure they are all tightly coupled to the ground and recording usable data. The spacing between them must be sufficiently small to correlate phases on adjacent traces and to obtain the desired resolution. Care is also needed in obtaining appropriate signals from the source, that is, making sure that the source signal is clean. For example, care is needed in avoiding a double strike of the hammer or a ringing record. The best shot for each station was chosen, based on these factors. The principal deficiency in this survey is likely related to using a maximum fold of 4, resulting in a maximum increase of 200% in the signal/noise ratio.

The seismic profile for Transect 3 can be seen in Figures 3.1-3.4. Though few reflectors are apparent, two main features, the soil/bedrock interface and the main fracture zone, can just be distinguished. In Figures 3.2 and 3.4, the top of the bedrock comes up from 5.5 to 7 m towards the surface, then beyond 7 m it gently slopes down, before flattening out. In contrast, the main fracture zone, begins flat, before gently sloping up to meet the soil/bedrock interface at 15 m. This same structure can be seen in the corresponding reflectors in the GPR image of Transect 3 (Figures 3.7 and 3.8). The fractures are referred to fracture zones, because in nature, fractures rarely occur singularly, but rather in groupings. This will be discussed in more detail in the following chapter. In Figure 3.2, it can clearly be seen that these reflectors have the highest amplitudes from 5.5 -9.5 m along the profile. This area corresponds to the closest geophone spacing (5 cm) and highest fold (4) data. Although the maximum coherent amplitude is only 2 times greater than the noise, these a higher amplitude arrivals can be related to structure.

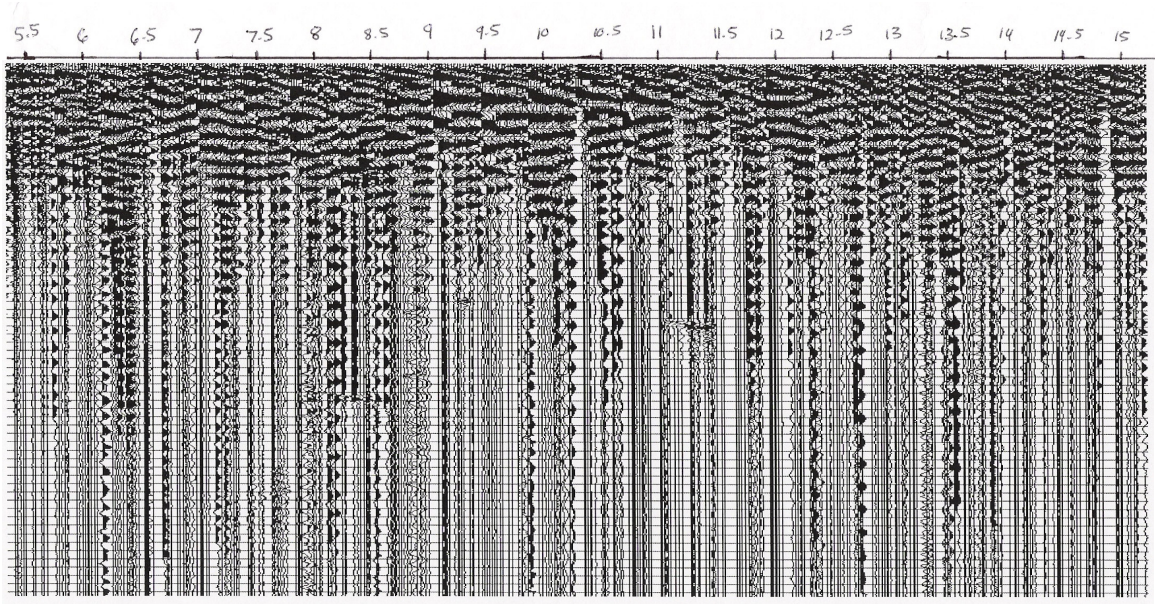

Figure 3.1 The raw, unstacked SSR data.

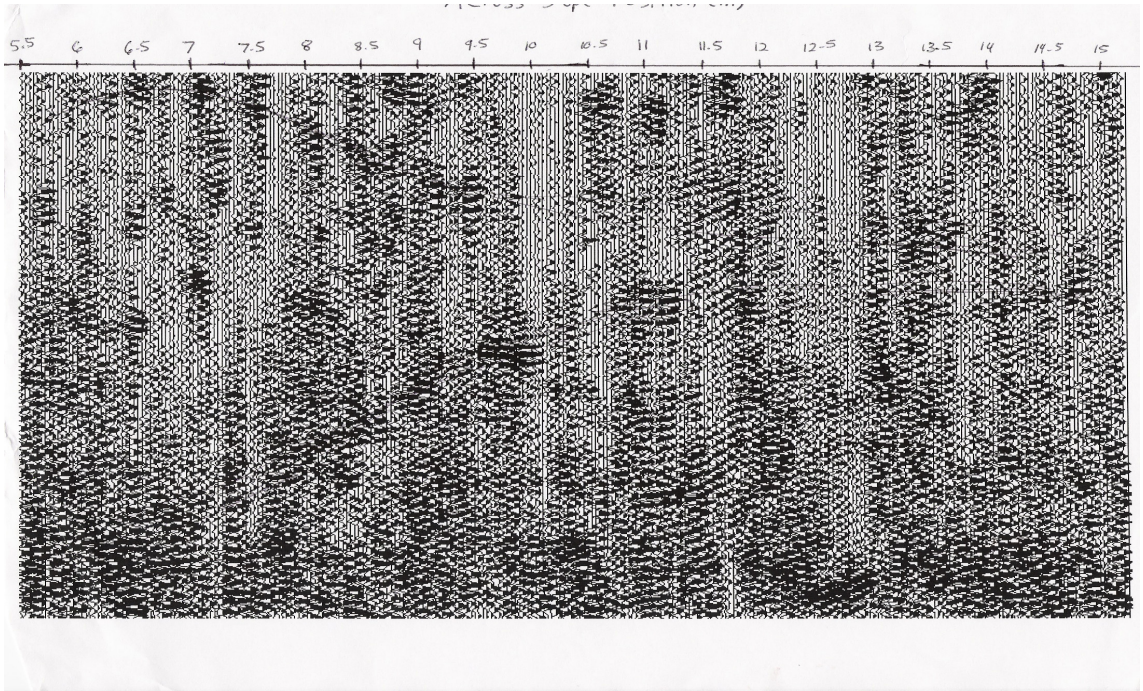

Figure 3.2 Bitmap image of the completely processed and stacked SSR profile. It is easier to see the reflectors in this image than in the standard print section (Figures 3.3 and 3.4). Notice the shallow, high amplitude area close to 11.5. This is close to the object labeled H1 in the corresponding GPR profile (Figure 3.7). It could be an erosional remnant.

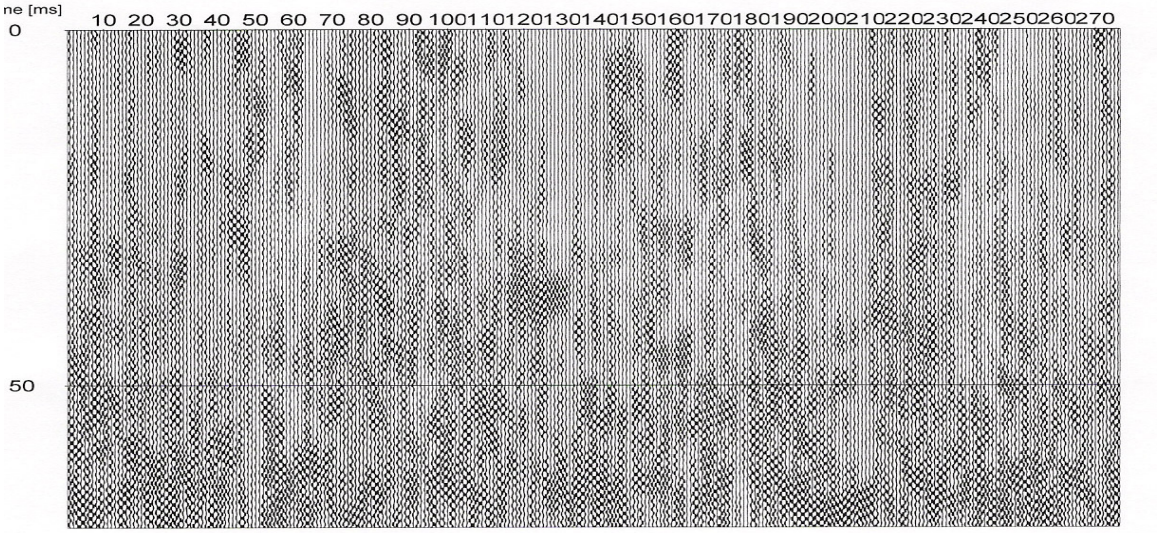

Figure 3.3.a A standard print section of the SSR profile. Note the zones of higher amplitude coherence. By comparing this image to Figure 3.6, one can make out the soil/bedrock interface and the main fracture zone. The horizontal axis is the CDP number, and the vertical axis is travel time (ms).

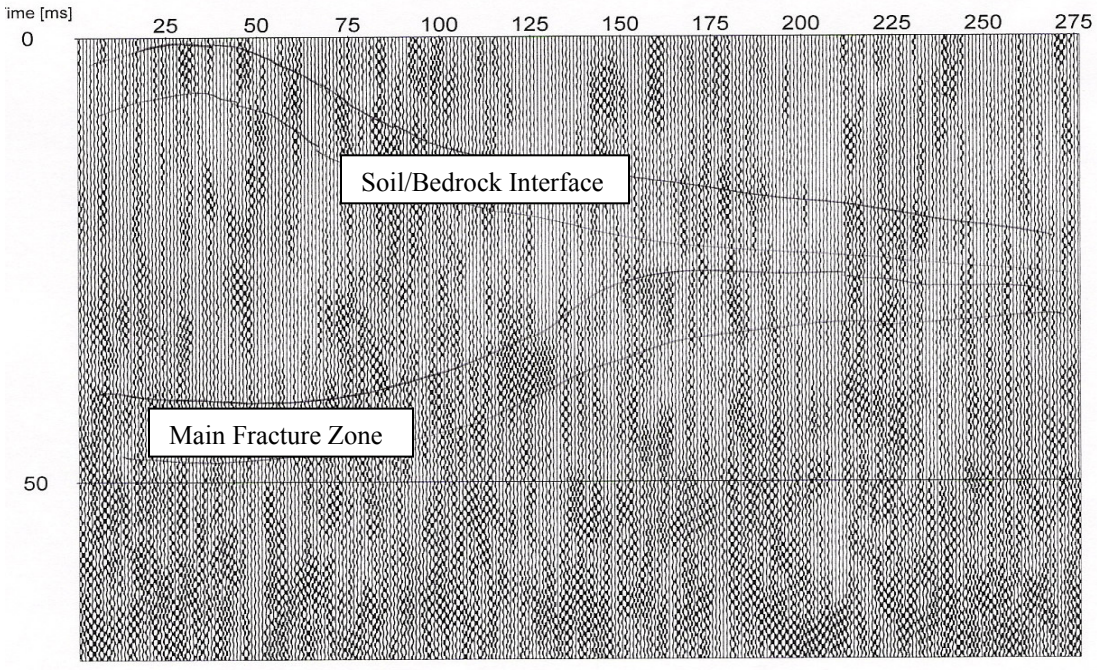

Figure 3.3.b A standard print section of the SSR profile. Here, lines have been drawn in where the reflectors should be.

Resolution in seismic reflection data is the minimum arrival time difference needed to differentiate two reflectors. The vertical resolution in seismic surveys is generally obtained by using the quarter wavelength approximation (Baker et al., 1999). This states that the minimum vertical resolution is proportional to one-fourth the wavelength of the seismic wave in the medium. The wavelength is related to the velocity and frequency of that medium.

$$v = f\lambda \tag{3.1}$$

Thus, if the velocity is known for a given medium, as well as the dominant frequency, the wavelength can determined, thus giving the vertical resolution. The dominant frequency of reflection in this study, was determined by measuring a period of 4m/s (f = 250 Hz) on the soil/bedrock reflector at 13 ms in Figures 3.4 and 3.5. Then using the mean soil velocity of 428 m/s and an average bedrock velocity of 1410 m/s (both values determined through the refraction survey, which will be discussed later), then the wavelength in the soil is 1.7 m and 5.6 m in the bedrock. If the quarter-wavelength is indeed a good approximation of vertical resolution (Baker et al., 1999), then the vertical resolution is 0.4 m in the soil and 1.4 m in the bedrock. Compared to standard production reflection surveys (Dobrin, 1976), the values in the soil are 1900 - 3800 % smaller than the 7.5-15 m obtained, but are 200-400 % larger than the 0.1-0.2 m obtained in other SSR surveys conducted (Baker et al., 1999; Baker et al., 2001). When the seismic source generates a pulse, the wave does not reflect off a singular point on the reflector, but from a small area known as the footprint. The footprint, which expands over time, can be approximated as a circle of radius a, with the point of incidence at the center. This radius, which is given by Equation 3.2, is the lateral resolution (Elachi, 1987).

$$a = [v(t/f_c)^{1/2}]/2 \quad (3.2)$$

Using Equation 3.2 to solve for the lateral resolution gives a value of 1.2 m at 10 ms in the soil, and 9.5 m at 45 ms in the bedrock. While this resolution would be quite acceptable for a standard prospecting transect that is 5000 m long, it is poor for the much smaller scale encountered in SSR surveys. For instance, the SSR profile obtained in this survey is only 10 m long, so the ratio of the lateral resolution to length of the profile is 0.12 for the soil and 0.95 for the bedrock. This explains the lack of clarity in the seismic profile. However, because there is amplitude coherence in the same pattern as those zones found in the GPR image of Transect 3 (Figures 3.6 and 3.7), it can be said that SSR is capable of detecting the top of the bedrock and the main fracture zone.

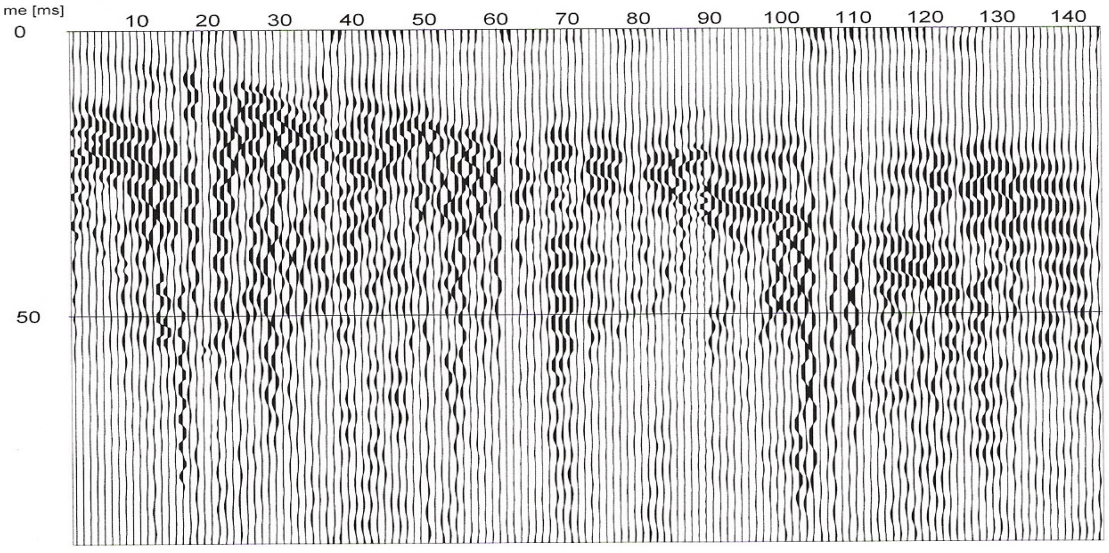

Figure 3.4 A CSP survey for Transect 2 filtered with a 100-650 Hz band pass filter. Notice the reflection off of the soil/bedrock interface at around 13 ms.

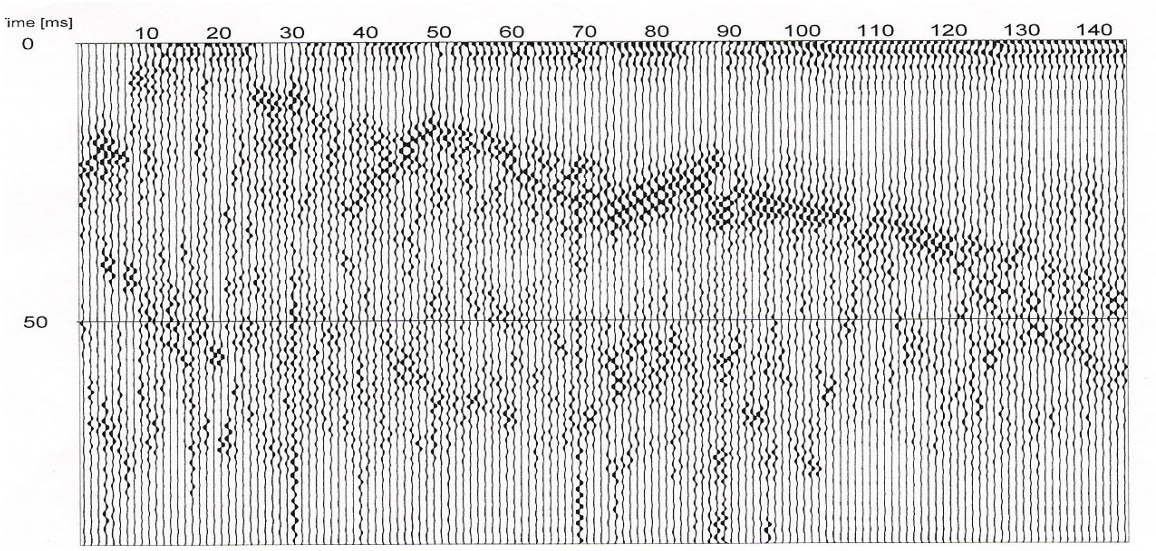

Figure 3.5 The same CSP survey of Transect 2, but this figure was filtered with a 300-800 Hz band pass filter. The backscattering around trace 80 (8.5 m actual) are due to lateral heterogeneities such as a boulder. This corresponds to the bedrock surface roughness and the diffraction hyperbola remnants seen between 8 and 8.5 m (actual distance) along Transect 2 as seen in Figure 3.13.

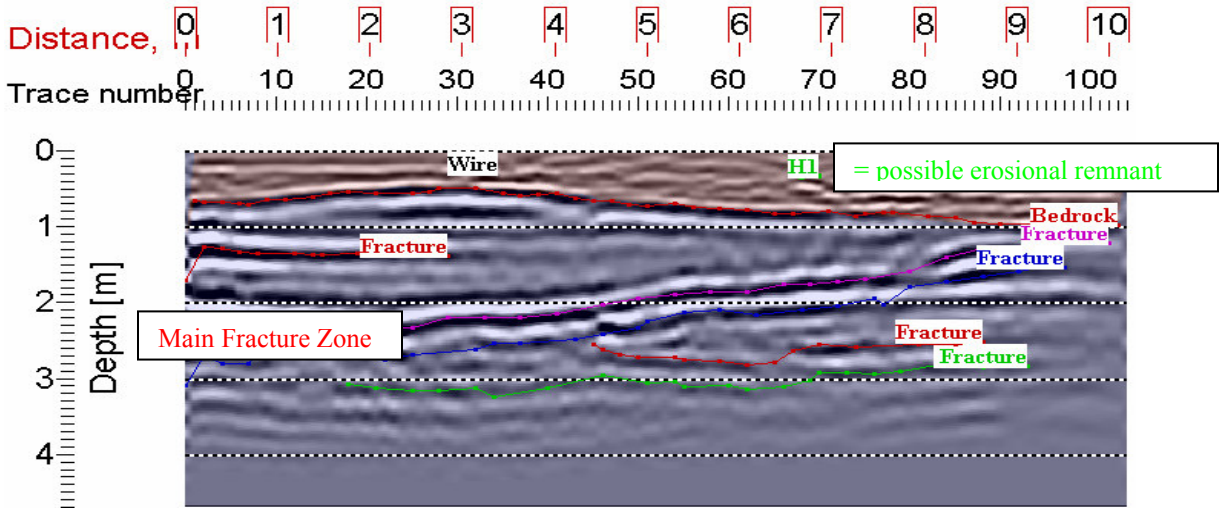

Figure 3.6 A GPR image of Transect 3 in grey scale format (3 m upslope from trench). The soil/bedrock interface is visible at about 1.0 m, as converted using the velocity model determined. Some likely planar fracture zones are indicated. Note how the main fracture zone intersects the top of the bedrock at 14.5 m along the transect at 1m converted depth. The bright spot labeled H1, is a diffraction hyperbola that has been compressed down to a singular point at the apex using Stolt F-K migration (possibly a boulder). Also, the actual transect runs from 5.5 m-15.5 m.

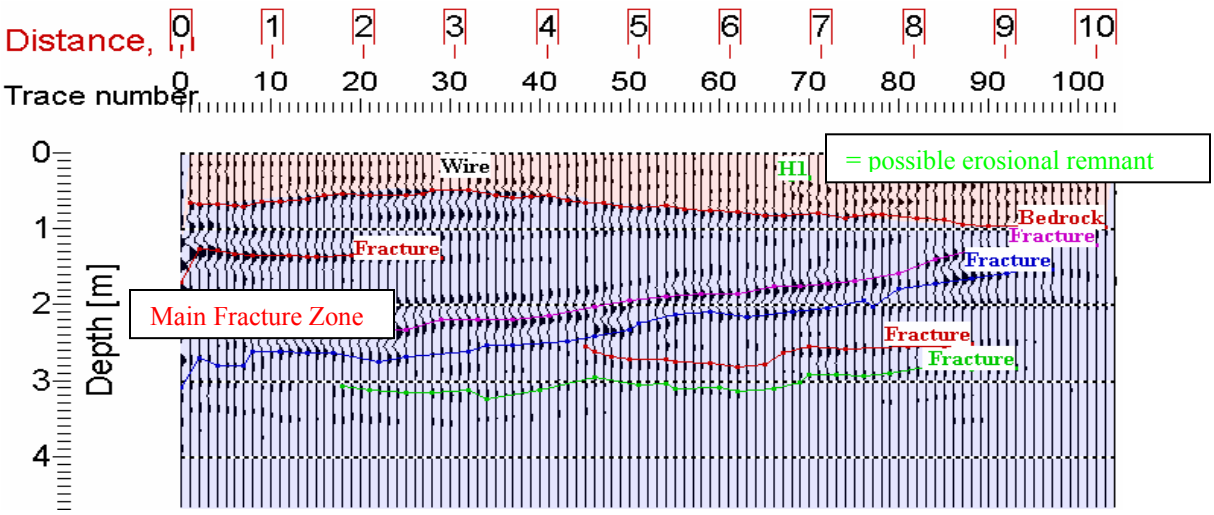

Figure 3.7 A GPR image of Transect 3 in variable amplitude format (3 m upslope from trench).

The ground truth included two knocking pole surveys. The first was obtained in 1998 by Zumbhul, and the second conducted specifically for this study (Figures 1.2-1.5, Tables 1.1 and 1.2). The knocking pole surveys determine the depth to bedrock by pounding a steel rod until refusal. The depths to bedrock from the knocking pole survey were found to be shallower than the times converted to depths for points on the interpreted soil/bedrock interface, from the SSR profile (Figure 3.8). Using the mean velocities determined from the refraction study (428 m/s for the soil and 1410 m/s for the rock), results in points on a profile that are 2 to 12 times deeper than those determined in the knocking pole survey (Figures 1.6). Because these differences varied in proportion to depth (Figure 3.9), the inconsistency is attributed to incorrect velocity values. In the soil, it could be due to lateral velocity inhomogeneities from boulders or tree roots, speeding up the apparent velocity of the soil, which is an average over the entire length of the transect. For instance, if the boulders are detached pieces of the Panola granite (5500 – 6300 m/s) in the soil (375 – 481 m/s), then for the width of the boulder, the P wave would

be traveling anywhere from 11 – 17 times faster than in the rest of the soil. The strong heterogeneity makes the determination of velocity highly variable along the path, resulting in incorrect depths. Of course, another possibility is that knocking pole survey could represent some of these shallower rocks, giving a false indication of the depth of weathering.

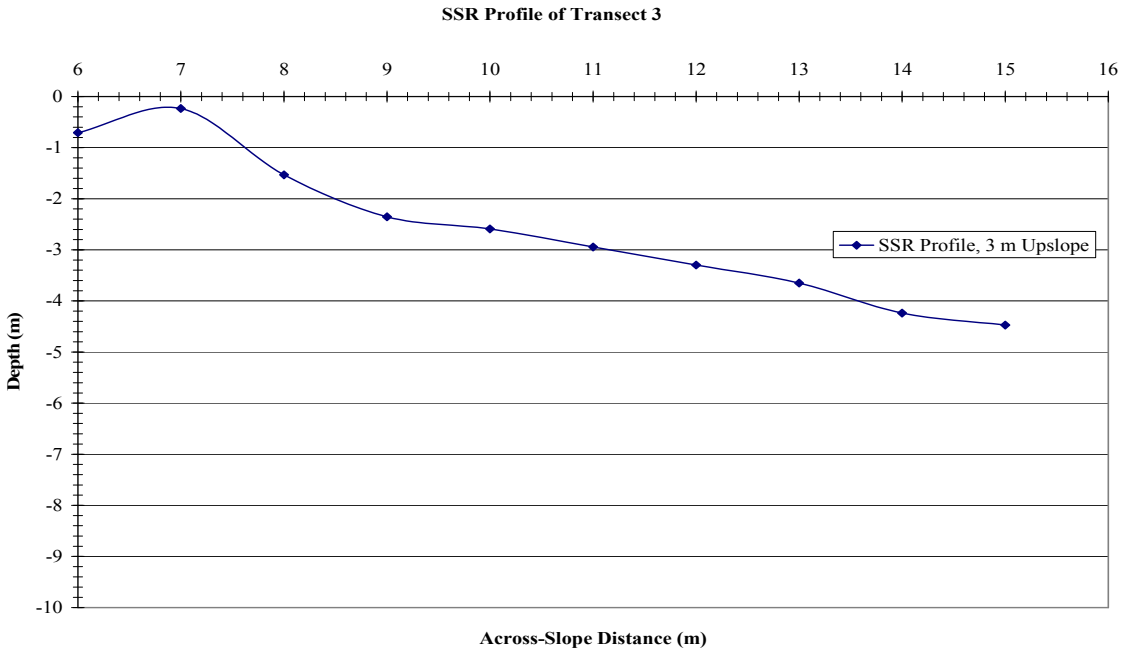

Figure 3.8 A depth profile of the SSR survey, converted using the soil velocity determined from the refraction study, and travel times picked from Figure 3.3.b

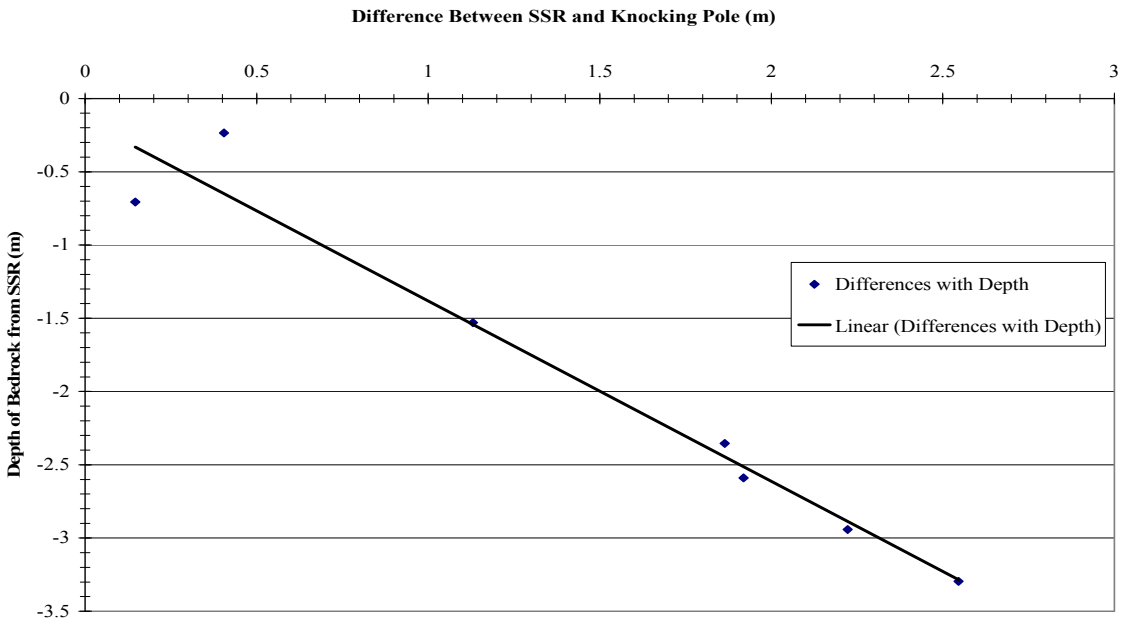

Figure 3.9 Offset versus depth between the SSR and knocking pole surveys. The increase in vertical offset with depth suggests incorrectly determined velocity values.

3.2 Ground-Penetrating Radar

The GPR survey imaged the main fracture zone (Figures 3.6 and 3.7, 3.10-3.15) and some of the smaller horizontal fracture zones as well. Also, the GPR located the soil/bedrock interface on each of the four transects (Figures 3.6 and 3.7, Figures 3.10-3.15), including the weathered areas. The interfaces imaged in the GPR profile of Transect 3 were similar to those obtained in the SSR survey (compare Figure 3.7 to Figure 3.2). Likewise, the soil/bedrock interface was nearly identical in shape to the results of the knocking pole survey of Transect 3 (Figure 1.6), deviating in depth only by an average of 11cm.

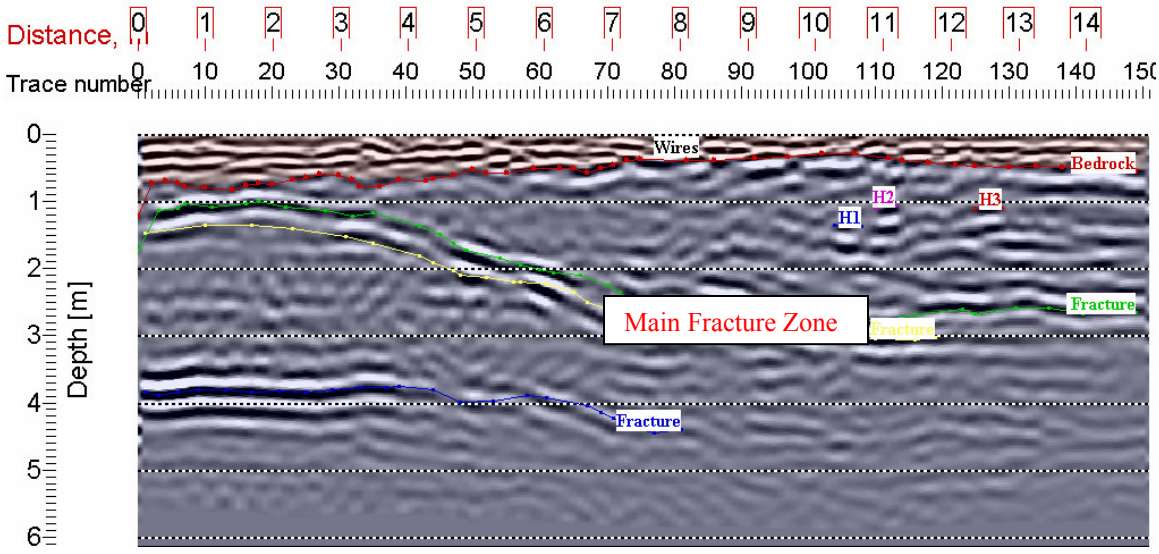

Figure 3.10 A GPR image of Transect 1 (20 m upslope from trench) in grey scale format. The soil/bedrock interface is clearly visible, as well as several planar fracture zones. The bright spots labeled H1, H2, and H3 are diffraction hyperbolas that have been compressed down to a singular point at the apex using Stolt F-K migration. The actual transect runs from 4 m-19 m.

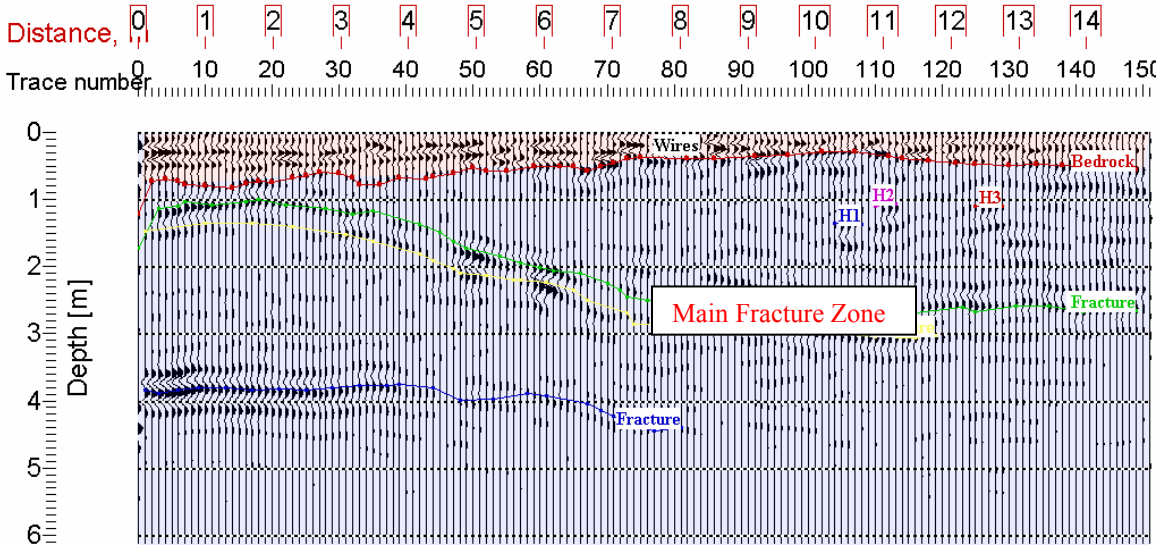

Figure 3.11 A GPR image of Transect1 (20 m upslope from trench) in variable amplitude format.

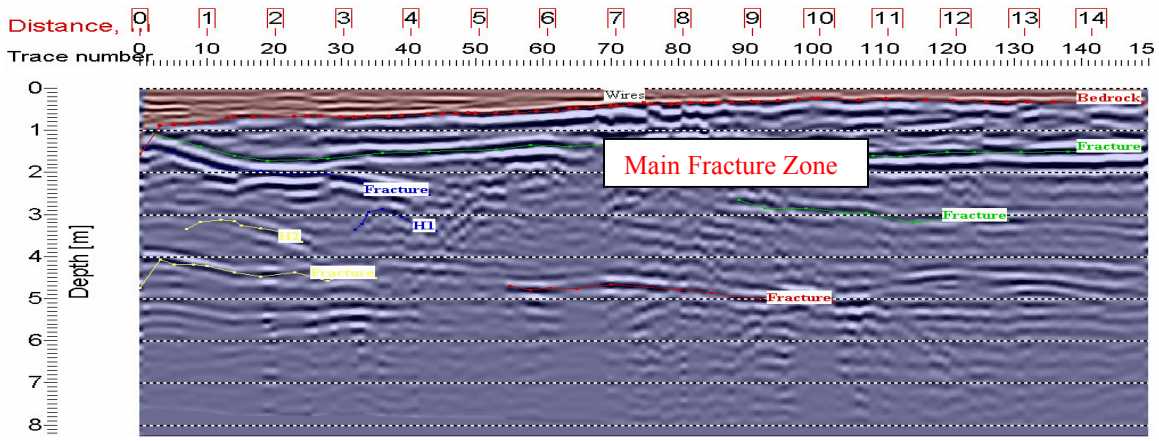

Figure 3.12 A GPR image of Transect 2 (11.4 m upslope from trench) in grey scale format. The soil/bedrock interface are clearly visible, as well as several planar fracture zones. One of these zones intersects the soil/bedrock interface at 1 m depth. This transect was taken almost exactly where the Bromide line tracer was released (11m upslope from trench). The bright spot labeled H1 is a diffraction hyperbolas that have been compressed down about the apex using Stolt F-K migration. The remnants of several other diffraction hyperbolas, caused by several wires on the ground, can also be seen. The actual transect runs from 0.5 m-15 m.

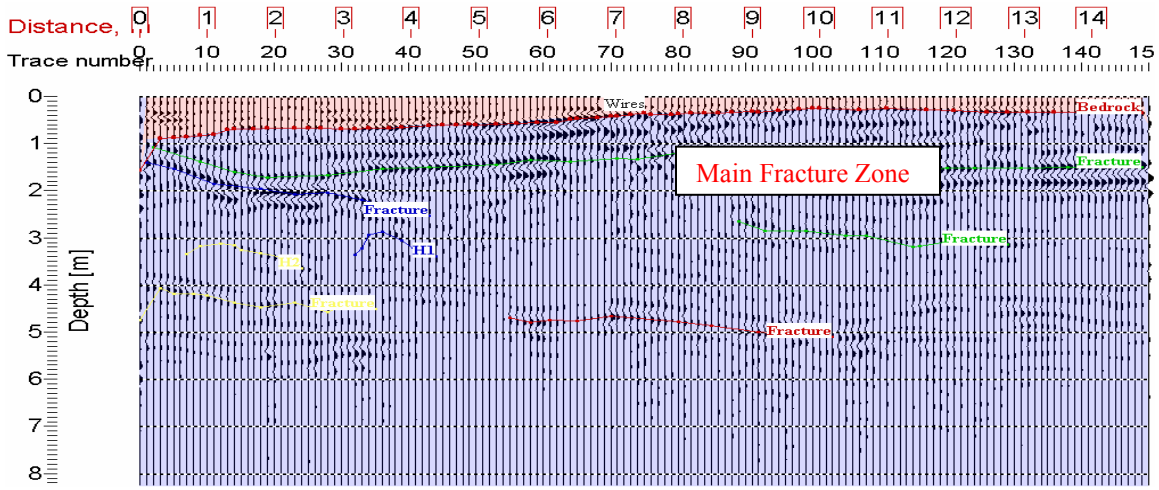

Figure 3.13 A GPR image of Transect 2 (11.4 m upslope from trench) in variable amplitude format.

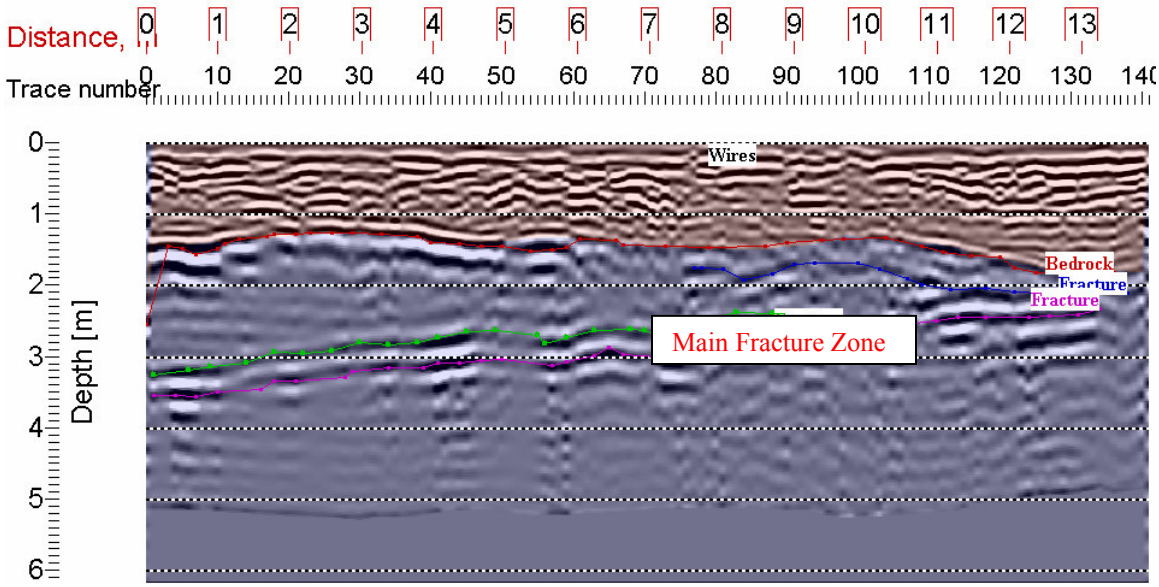

Figure 3.14 A GPR image of Transect 4 (4 m down slope from trench) in grey scale format. One will notice that the soil/bedrock interface is not as clearly defined as in the previous three profiles. The fuzzy area could be a highly weathered zone. However, despite this, the major fracture zone can still be seen. The remnants of diffraction hyperbolas can still be seen due to surface wires. This transect is laterally correct.

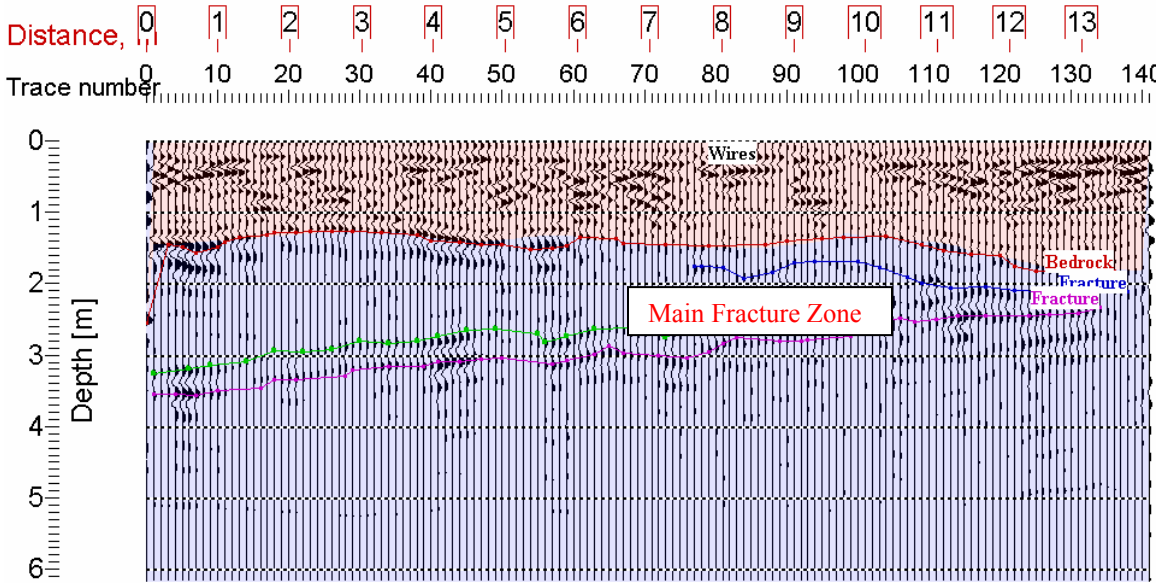

Figure 3.15 A GPR image of Transect (4 m down slope from trench) in variable amplitude format.

The dielectric constants of the two media were found using a diffraction

hyperbola fitting routine in Rad Explorer. The dielectric values calculated by the routine were $K_s = 8$ for the soil and $K_{br} = 14$ for the bedrock. These values fall into the range of values for soil and granite given in Clark (1966). Their position within these ranges will be discussed in the following chapter. Using Equation 2.11, these values gave velocities of $1.0*10^8$ m/s for the soil and $8.0*10^7$ m/s for the bedrock. These velocity values, along with the center frequency of the antenna used ($2.5*10^8$ Hz) can then be used to determine the lateral and vertical resolution. In GPR surveys, ½ wavelength approximation is used for the vertical resolution (Parasnis, 1997). By using Equation 3.1 to determine the wavelength, the vertical resolution is determined to be 0.2 m in the soil and 0.16 m in the bedrock. Equation 3.2 is used to calculate a lateral resolution. At a time of 10 ns in the soil, the lateral resolution is 0.32 m, whereas at 45 ns in the bedrock, the resolution is 0.54 m. Thus, for Transect 3, which has a length of 10 m, the ratio of the lateral resolution to length of the profile is 3.2% for the soil and 5.4% for the bedrock.

The knocking pole survey estimated depths were used to compare against the GPR depth estimates. According to Equation 3.2, the GPR was able to image the structure of the interface, with about 200% finer lateral resolution than the knocking pole survey conducted for this study (0.5 -1.0 m) and 625% finer than the Zumbuhl (1998) survey (2 m). However, once again the depths calculated from the velocity model differed from the actual values determined from the knocking pole survey along Transects 2 and 3. On Transect 2 (Figures 1.5 and 3.12), the GPR depths were an average of 0.34 m too deep. On Transect 3 (Figures 1.6 and 3.6), the GPR depths were 0.11 m too deep on average. This could be the result of several things. First, the zero time might have been set incorrectly. This would cause a time shift, which would add a

constant to the depths. Second, the radar velocities could be incorrectly determined. Because there was interference between the reflected and diffracted waves, the diffraction hyperbolas were slightly distorted. By plotting the depth to bedrock from the GPR against the depth to bedrock from the knocking pole surveys (Figure 3.16), one can see that there is not a uniform increase in the difference with depth as with the SSR survey. For this reason, this deviation from the known values was interpreted as an incorrectly chosen time zero, or a combination of that and an incorrect radar velocity for the soil. Still, despite this issue, it is apparent that ground penetrating radar can image the bedrock and some fracture zones.

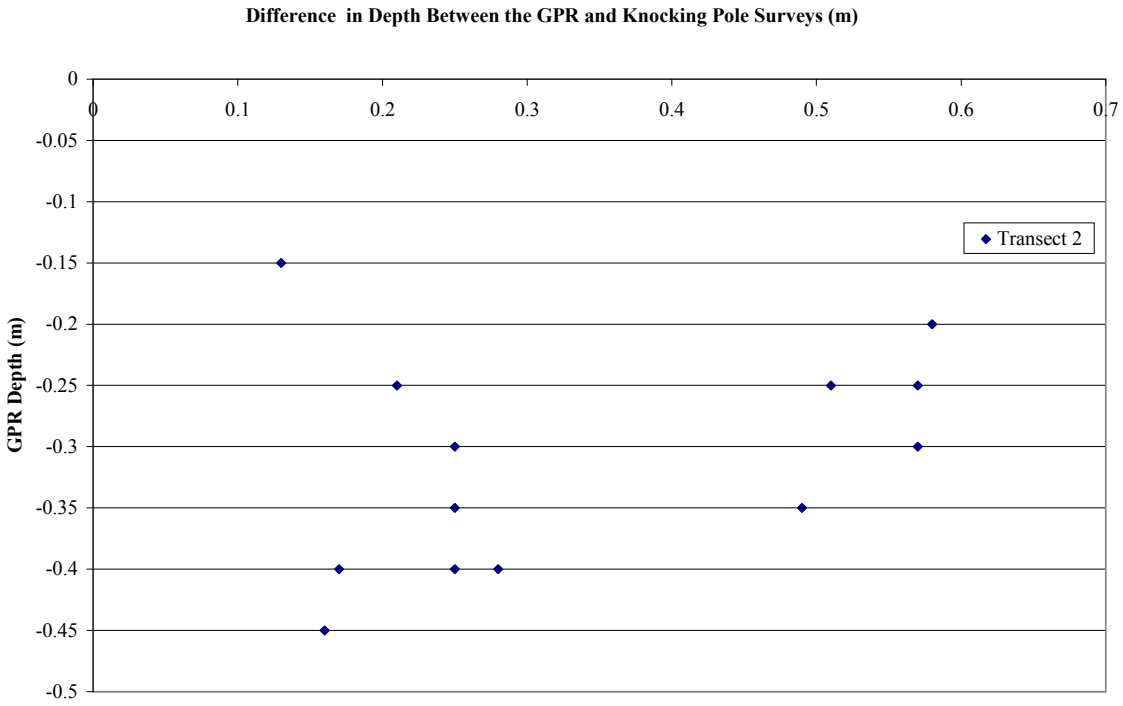

Figure 3.16 The deviation between the radar and knocking pole surveys with depth.

3.3 Shallow Seismic Refraction

Although shallow seismic refraction is not appropriate for imaging fracture zones, it is able to generate an image of the bedrock topography for a 4m section of Transect 2 (Figure 3.17). Also, the common shot point (CSP) surveys taken of Transects 2 and 3 allowed a velocity value to be calculated for both the soil and the bedrock. After plotting the first arrival times versus offsets for these surveys (Figure 3.18 and 3.19), a linear regression analysis was run on the data points corresponding to the lower velocity layer and another on those corresponding to the faster layer, for each transect. From that analysis, the best-fit soil and bedrock velocities from those transects were then averaged, and their standard deviations calculated. Through this process, the average velocity value for the soil was 428 ± 53 m/s. Likewise, the average velocity calculated for the bedrock was 1410 ± 337 m/s.

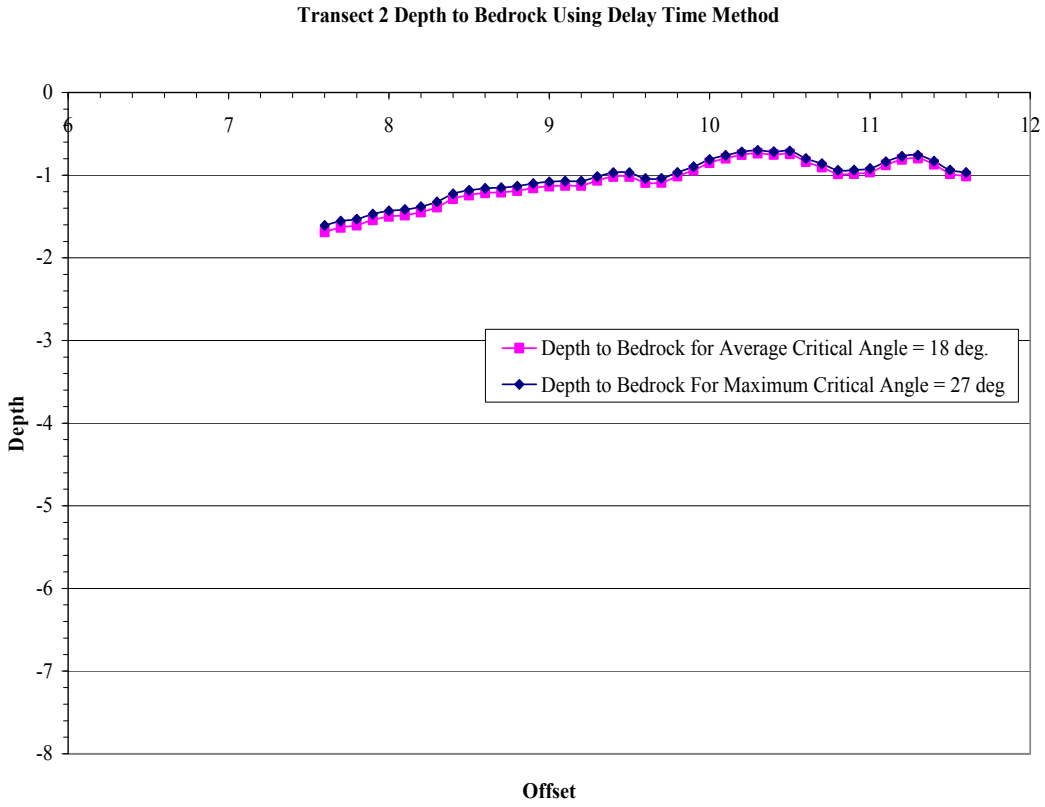

Figure 3.17 Computation of the soil-bedrock interface for Transect 2 from the Delay Time Method. The horizontal axis is distance from the beginning of the trench. One can compare this to the GPR image of Transect 2 in Figure 3.13 and see they are very similar. The mean vertical offset between the two models is 5 cm. These are the refraction depth to compare with the knocking pole survey.

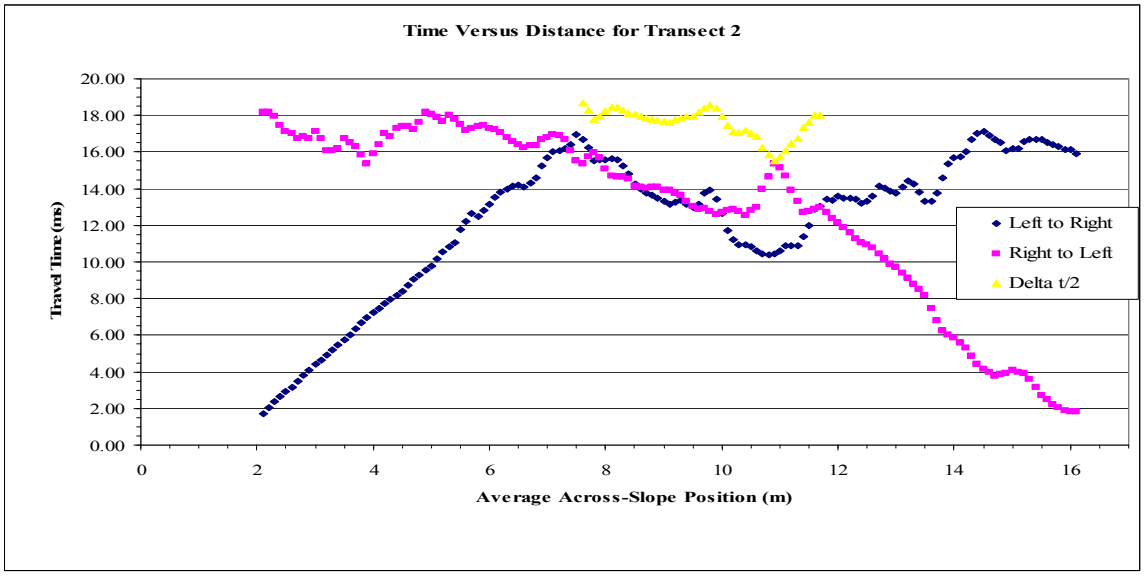

Figure 3.18 First arrival times are plotted versus offset for Transect 2. One will notice a clear point where the slopes of the lines change. This is the critical point (x_c). The steeper slope is the direct wave, the inverse of which is the velocity of the upper layer, in this case, the soil. The shallower slope is the refracted wave, the inverse of which is the velocity of the bottom layer.

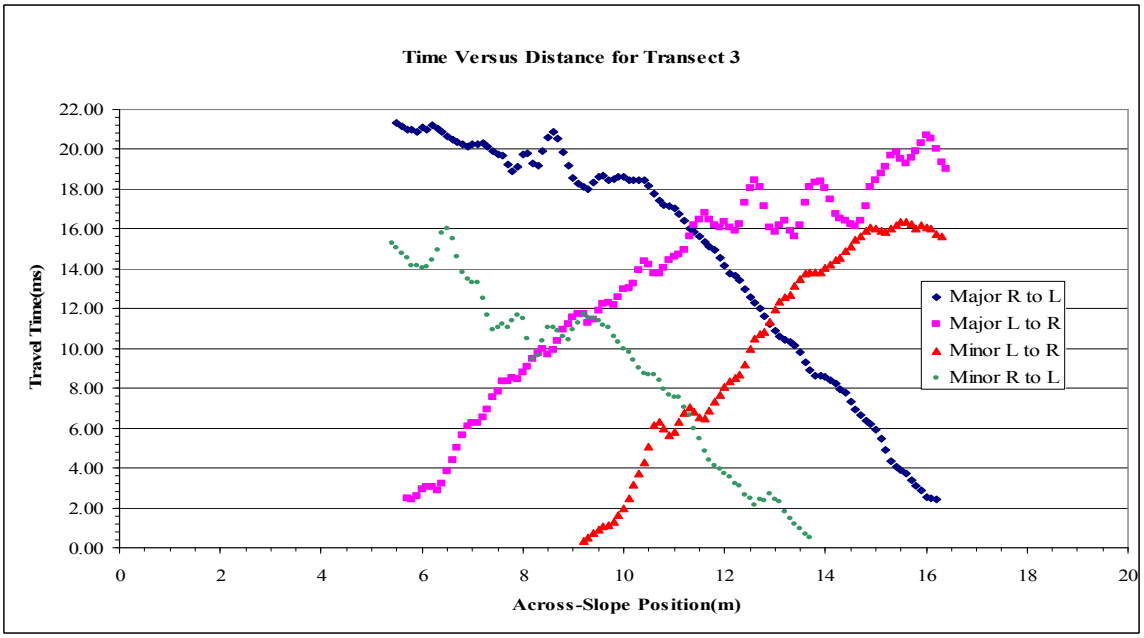

Figure 3.19 First arrival times are plotted versus offset for Transect 3. The travel times and offsets were averaged to decrease the variability. The critical points are obvious, but because they overlap, the Time Delay Method could not be used to generate an image of the soil/bedrock interface (in text).

The soil exhibits a slow velocity because it is a loosely packed, sandy, colluvial loam (Zumbuhl, 1998) giving it a lower density and even lower elastic constants. Also, it is overlain by a 0.15 m thick layer of humus, which would slow down the mean velocity. The measured value for the bedrock is also slow, more than likely because the refraction from the deeper bedrock surface was not observed. The observed velocity is most likely from a thick layer of either saprolite or water-saturated soil directly on top of the bedrock. We know the velocity of the hard rock should be 4900 to 6100 m/s, significantly greater than the measured 1410 m/s, and not fast enough to be sedimentary, non-ripable rock at 2400m/s (Touloukian and Ho, 1981). If the layer is composed of saprolite, then this is in direct contradiction to Burns et al.(2003) who said that there was no saprolite in this area. One possibility is that this area has a hidden thick saprolite weathered zone, but this is unlikely considering the lack of saprolite seen on the outcrops. It is also unlikely, because the weathering front moves very slowly in the Panola granite (at only 7 m per million years) (White et al., 2001). The more likely possibility, is that the observed P-waves were actually refracted from a thin saturated zone directly on top of the bedrock. This possibility is consistent with the pre-determined velocity (1410 ± 337 m/s) , which is very similar to the velocity of water, which is approximately 1500 m/s. However, by comparing the 7 - 11.4 m section of the GPR profile of Transect 2 (Figure 3.12) to the image of bedrock topography (Figure 3.17), one can see that they are nearly identical in structure. This implies that the thin saturated layer closely follows the bedrock topography. This fact is consistent with Freer et al. (2002). Another possibility is that the interface between the high-velocity rock and the soil/saprolite is too irregular to support propagation of a high-speed refracted wave. The refracted wave in the

unweathered Panola granite is likely highly scattered and without sufficient amplitude to be observed at the surface.

The bedrock topography calculated from the time-delay method (Figure 3.17) matches the ground truth in shape, except once again, for the magnitude of the depths. The depths calculated by the Delay Time Method (Equations 2.19 and 2.20) are deeper than the knocking pole values (Figure 1.4) by 0.09-1.4 m. Because the offset between the calculated values and the actual value from the knocking pole survey varies continuously with depth (Figure 3.20), this discrepancy is probably due to velocity that is too fast. Figure 3.18 shows the values determined for two different critical angles. One can see that there is very little difference between the two (the mean offset is 5 cm), because Equation 2.20 is mostly controlled by the velocity of the upper layer.

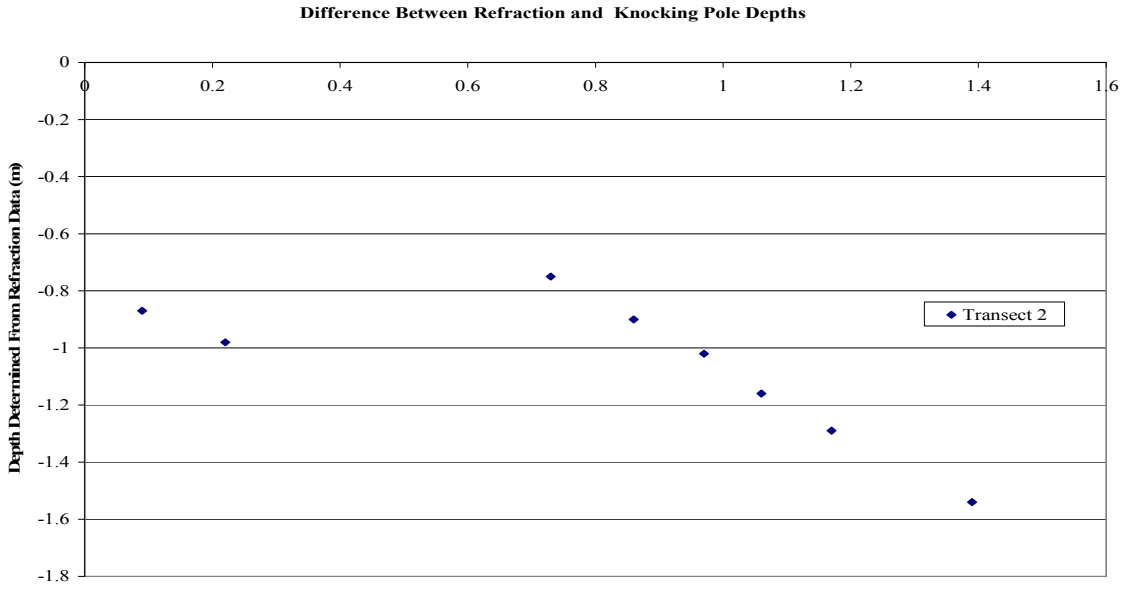

Figure 3.20 The difference between the knocking pole survey and the profile determined from the Delay Time Method. Although there is an offset between point 2 and point 3, the increasing difference with depth trend is clear.

The results of this study are summarized in Table 3.1. Both the SSR and the GPR were able to provide images of the fractures, but the GPR had higher resolution. The next chapter will discuss the results in greater detail, specifically the velocity values determined, and the relationship between the features identified and the hidden hydraulic pathways originally mentioned.

Table 3.1: Comparison of results for techniques used.

	Soil Velocity (m/s)	Bedrock Velocity (m/s)	Imaged Bedrock ?	Imaged Fracture Zones?	Vertical Resolution (m)	Lateral Resolution in Soil (m)	Lateral Resolution in Rock(m)
SSR	428	1410	Yes	Yes	0.4-1.4	1.2	9.5
GPR	1.0 E8	8.0 E7	Yes	Yes	0.16-0.2	0.32	0.54
Shallow Seismic Refraction	428	1410	Yes	No	x	0.32	x

Chapter 4

Discussion

From the previous section, there are two issues that require further discussion . The first concerns the differences in depth determination, most likely due to the uncertainty in the velocities. The second concerns the association between the interpretations of structure and hidden hydraulic fractures.

The interpretations of depth differed significantly among the SSR, GPR, seismic refraction, and knocking pole surveys. For the GPR profiles, the vertical offset was mostly constant with depth, indicating a misplacement of the zero reference time. However, for the seismic profiles, the differences in depths were determined to be due to systematic differences between reflection and refraction velocity values.

The seismic velocity of the soil was determined to be slow, 428 ± 28 m/s. This soil was described to be a loosely packed, sandy, colluvial loam; overlain by an average layer of 0.15 m humus (Zumbuhl, 1998; Tromp-van Meerveld, 1998). The speed of sound in air at (1atm), at 20°C is 343 m/s (Haliday, Resnick, and Walker, 1997). Thus, it is implied that a soil having a velocity 88-116 m/s faster than the acoustic wave in air would consist of very loose particles, surrounded by air. This is descriptive of the humus layer. In reality, acoustic velocities for sediments similar to those encountered in this study were actually slower than the speed of sound, ranging from 130 -300 m/s (Baker et al., 1999). However, the soil was damp during the surveys performed in this study, which would increase the seismic velocity in slow soils. This dampness is consistent with the GPR data. For the GPR survey, the dielectric constant of the soil (K_s) was found

to be equal to 8, resulting in an EM velocity of $1.0*10^8$ m/s. According to Clark (1996), the dielectric constant of a dry, loamy soil is only 2.6. However, for a soil that is 32% saturated, K_s is 7.93. So, a slow, loamy soil that is partially saturated, averaged with a thin, loosely packed layer of humus, would give a soil velocity similar to the one determined.

The bedrock velocity determined from the seismic refraction survey was 1410 ± 337 m/s. This velocity is much too slow, even for fractured granite. The explanation given was that the refracting layer observed was actually a thin, saturated layer of soil, directly on top of the bedrock. The acoustic velocity of water at sea level with a temperature of 20°C is 1460 m/s (Haliday, Resnick, and Walker, 1997). This is very similar to the actual value, implying the refractor is indeed, a saturated layer. Unfortunately, this means that the true P-wave velocity of the bedrock was not determined. Perhaps too little energy penetrated into the high velocity refractor. However, the EM velocity of the bedrock was determined. Using the determined dielectric constant (K_{br}) of 14, the velocity was calculated to be $8.0*10^7$ m/s. According to Clark (1966), the range of dielectric constants for granite is 4.8 – 18.9, resulting in an EM velocity range of $1.4*10^8 – 6.9*10^7$. Because the dielectric constant of water is equal to 80, that implies that the higher the water content within the rock, the higher the dielectric constant, and the slower the EM velocity. Because the granite is said to contain fractures that transmit fluid (Tromp-van Meerveld, in review), the radar velocity calculated is quite reasonable. This velocity value helps confirm the existence of fractures in the Panola granite beneath the trenched hillslope study site.

The second issue is the relation between the interpretations in this study and the hidden fractures at the PMRW. The main objective of this thesis was to determine if SSR can be applied to locate fractures. Within the bedrock, the four GPR profiles showed horizontal reflecting features that extend the entire length of the profile, as well as several smaller horizontal discontinuities that extend half of the length. The SSR profile of Transect 3 shows two bands of higher amplitude arrivals in the same areas as the corresponding GPR profile. The upper band of high amplitudes is interpreted as the soil/ bedrock interface. The lower band is the proposed fracture zone. However, without direct observation, it is impossible to say for sure that these features are fracture zones. There are several factors that suggest that they are fractures. First, while other types of lateral heterogeneities can give reflections, they would not produce a full-length reflection, as a fracture would. Second, the EM velocity of the bedrock implies that these are fractures. Finally, fractures can be seen at the surface on the adjacent outcrop, so it is probable that there are fractures below the surface of the test site as well. These three factors imply that the reflectors in the bedrock imaged by the SSR and GPR techniques, are fracture zones.

Given that the SSR and GPR techniques imaged the fractures, several points can be made. The first relates to fracture genesis. By observing the slabs separated from the outcrops, the predominant form of fracturing in the Panola granite is exfoliation. This is consistent with the nearly planar, gently sloping radar images of Profiles 2, 3, and 4 (Figures 3.6 and 3.7, Figures 3.12 – 3.15), but not with the irregular, steeply sloping fracture of Profile 1 (Figures 3.10 and 3.11). Although a definite solution to the irregular shape of Profile 1 is not available at this time, it could be related to a thermal issue, such

as the repetitive diurnal thermal expansion and contractive cooling, or maybe it could be due to frost wedging. However, regardless of how the fractures were formed, they were imaged. The second point relates to how the fractures were imaged. On all of the radar profiles, the reflectors said to be fractures all have at least two reflecting interfaces. These interfaces could be the top and the bottom of the fracture, or they could be two fractures in a zone of fractures. In the previous section, it was determined that the vertical resolution of the GPR was 0.16 m in the bedrock. This means that for the main reflections seen in the profiles to be considered one fracture, there must be a separation, or void, of 16 cm between fracture surfaces in the bedrock. While some exfoliation joints seen on the surface exhibit separations that are close to this thickness, it is unlikely that the fracture openings are that large. One reason for this unlikelihood, is the amount of fluid being measured in the bedrock. Tromp van Meerveld et al. (in review), measured a hydraulic conductivity of 120 m per year in their Lithium - Bromide line tracer experiment. While this is much faster than the 7 m per million years determined by White et al. (2001) in their evaluation of Panola granite cores, it is not even close to the meters per second of flow that would occur through a 16 cm fracture, unless it was filled with weathered rock. It seems more likely that the second reflecting interface seen in the GPR profiles is actually due to a completely different fracture. If a 0.2 m thick section of bedrock had several fractures in it at least 0.16 m apart, two reflections would be generated the same as one very large fracture. For this reason, the fractures in this study have been referred to as "fracture zones." Finally, given that the fractures do indeed exist, and that they transmit fluid making them very important to the total hydrology of the study site, one might ask how the fractures access the water in the overlying soils?

One potential method is through vertical fractures from the soil/bedrock interface down to the horizontal fracture zones. Although no vertical fractures were imaged by any of the techniques used in this study, it does not mean that they are not there. However, what was imaged in this study, were lateral fracture zones gently slope towards the top of the bedrock, a characteristic of exfoliation joints. On the far left side (0.5 m) of the GPR profile of Transect 2 (Figure 3.12), the uppermost fracture zone is seen to intersect the top of the bedrock. Similarly, the SSR and GPR images of Transect 3 (Figure 3.2 and 3.6) show the shallowest fracture zone sloping up towards the bedrock surface, and potentially intersecting it at 15.5 m. The same can be seen at the end of Transect 4 (Figure 3.14). From these images, it is believed that the fluid infiltrates the bedrock through these zones.

Thus, based on the discussion given above, it should be clear that hidden hydraulic pathways do exist at the trenched hillslope site of the PMRW in the form of horizontal exfoliation fracture zones. From the data, it is apparent that GPR is a good tool for imaging these zones. However, if care is taken to insure the high frequency content of source energy, as well as maintaining small (5-10 cm) geophone spacing and higher fold (4 or greater), then SSR can also be a useful technique for imaging the horizontal fracture zones.

Chapter 5

Conclusion

This thesis has examined the application of shallow seismic reflection to a problem of locating fluid pathways in a hillslope. From this examination, several things can be concluded. First, that fractures are indeed present within the bedrock at the trenched hill-slope site of the Panola Mountain Research Watershed, and that they can be imaged using geophysical methods, specific to this study, ground penetrating radar. All four of the GPR profiles imaged a main fractures zone that extended across the entire length of the profile, as well as several of the smaller ones. The SSR survey of Transect 3 also imaged something where the main fracture zone was seen in the corresponding GPR profile.

The second conclusion, is that in SSR studies attempting to image fractures, GPR proves to be a better supplementary tool than shallow seismic refraction. Although seismic refraction was able to give a detailed image of the soil/bedrock interface for a portion of Transect 2, the refracted waves from the deeper, high-velocity layers could not be detected. This could be due to the smaller energy and lower frequency-generating source used, as well as the extreme velocity gradient. Had the transect been longer and had a more powerful source (or just one with the potential to generate higher frequencies) been available, deeper images might have been possible with this technique.

Finally, it can be concluded that more geophysical work; such as the GPR and SSR work done in this study, as well as other geophysical methods like borehole studies and electrical resistivity; should be done at the study site to better map the hidden

hydraulic pathways. A complete SSR survey could be conducted along all four transects, using a geophone spacing of 5 cm to get 400% coverage or greater. However, should this survey be planned, a higher frequency source must be used. Planned by these specifications, the survey would be successful in imaging the fractures. Another study that could be done, is comparing the reflection amplitudes of fractures imaged from GPR profiles using different polarizations. A 250 MHz antenna would be sufficient for this proposed study. This is done to determine the strike direction of the individual fractures (Seol et al., 2001). Also, a single borehole study could be performed along one transect to directly confirm fracture location and determine fracture density for the site, as well as providing direct measurements of the velocities. Because bedrock has a high resistivity, the conductive fluid pathways within the rock should be easy to detect.

These four studies, combined with the correct topographic data, could then be used to generate a 3-D map of the fracture network at this site. These suggestions are just a few of the numerous possible studies that could be conducted in the future. However, for the present, it is sufficient to see that geophysical methods, including SSR if done correctly, constitute a cost efficient way of mapping out hydraulic pathways in situ.

REFERENCES

Bachrach, R. and Nur, A. (1998). Ultra shallow seismic reflection in unconsolidated sediments: Rock physics for data acquisition. SEG Technical Publication.

Baker, G. S., Steeples, D. W., Feroci, M. (1997). The time dependence of shallow reflection data. *The Leading Edge* v. 16: 1663-1666

Baker, G. S., Steeples, D. W., and Schmeissner, C. (1999). In-situ, high-frequency P-wave velocity measurements within 1 m of the earth's surface. *Geophysics* v. 64: 323-325

Baker, G. S., Schmeissner, C., Steeples, D. W., and Plumb, R.G. (1999). Seismic reflections from depths of less than two meters. *Geophysical Research Letters* v. 26: 279-282.

Baker, G. S., Steeples, D. W., Schmeissner, C., Pavlovic, M., and Plumb, R. (2001). Near-surface imaging using coincident seismic and GPR data. *Geophysical Research Letters* v. 28: 627-630.

Bano, M., Edel, J. B., and Herquel, G. (2002). Geophysical investigation of a recent shallow fault. *The Leading Edge* v. 21: 648-650.

Benson, A. K. (1995). Applications of ground penetrating radar in assessing some geological hazards: examples of groundwater contamination, faults, cavities. *Journal of Applied Geophysics* v. 33: 177-193.

Black, R. A., Steeples, D. W., and Miller, R. D. (1994). Migration of shallow seismic reflection data. *Geophysics* v. 59 (3): 402-410.

Bohidar, R. N., and Hermance, J.F. (2002). The GPR refraction method. *Geophysics* v. 67: 1474-1485.

Burns, D. A., McDonnell, J. J., Hooper, R. P., Peters, N. E., Freer, J. E., Kendall, C., and Breven, K. (2001). Quantifying contributions to storm runoff through end-member mixing analysis and hydrologic measurements at the Panola Mountain Research Watershed (Georgia, USA). *Hydrological Processes* v. 15 : 1903-1924.

Burns, D. A., Plummer, L. N., McDonnell, J. J., Busenberg, E., Casile, G. C., Kendall, C., Hooper, R. P., Freer, J. E., Peters, N. E., Beven, K., and Schlosser, P. (2003). The geochemical evolution of riparian ground water in a forested Piedmont catchment. *Ground Water* v. 41 (7): 913-925.

Cardimona, S. J., Clement, W. P., and Kadinsky-Cade, K. (1998). Seismic reflection and ground-penetrating radar imaging of a shallow aquifer. *Geophysics* v. 63: 1310-1317.

Chow, J., Angelier, J., Hua, J. J., Lee, J. C., and Sun, R. (2001). Paleoseismic event and active faulting: From ground penetrating radar and high-resolution seismic reflection profiles across the Chihshang Fault, Eastern Taiwan. *Tectonophysics* v. 333: 241-259.

Clark, S. P. (1966). Handbook of Physical Constants. New York: The Geological Society of America, Inc.

Conyers, L. B. and Goodman,D. (1997). Ground Penetrating Radar: An Introduction for Archaeologists. London: Altamira Press

Cook, J. C. (1995). Preface. *Journal of Applied Geophysics* v. 33 (1): 1-3.

Derobert, X. and Abraham, O. (2000). GPR and seismic imaging in a gypsum quarry. *Journal of Applied Geophysics* v. 45: 157-169.

Demanet, D., Renardy, F., Vanneste, K., Jongmans, D., Camelbeeck, Theirry, and Meghraoui, M. (2001). The use of geophysical prospecting for imaging active faults in the Roer Graben, Belgium. *Geophysics* v. 68 (1): 78-89.

Dobrin, M. B. (1976). Introduction to Geophyscial Prospecting (3rd ed). New York: McGraw-Hill Book Company.

Elachi, C. (1987). Introduction to the Physics and Techniques of Remote Sensing. New York: John Wiley and Sons.

Freer, J., McDonnel, J. J., Beven, K. J., Brammer, D., Burns, D. A., Hooper, R. P., and Kendall, C. (1997). Topographic controls on subsurface storm flow at the hillslope-scale for two hydrologically distinct small catchments. *Hydrological Processes* v. 11(9): 1347-1352.

Freer, J., McDonnel, J. J., Beven, K. J., Peters, N. E., Burns, D. A., Hooper, R. P., Aulenbach, B., and Kendall, C. (2002). The role of bedrock topography on subsurface storm flow. *Water Resources Research* v. 38 : 1269-1285.

Ghose, R., Nijhof, V., Brouwer, J., Matsubara, Y., Kaida, Y., and Takahashi, T. (1998). Shallow to very shallow, high-resolution reflection seismic study using a portable vibrator system. *Geophysics* 63: 1295-1309.

Gueguen, Y. and Palciauskas, V. (1994). Introduction to The Physics of Rocks. Princeton: Princeton University Press.

Haliday, D., Resnick, R., and Walker, J. (1997). Fundamentals of Physics (5th ed). New York: John Wiley and Sons, Inc.

Jefferson, R. D., Steeples, D. W., Black, R. A., and Carr, T. (1998). Effects of soil-moisture content on shallow-seismic data. *Geophysics* 63: 1357-1362.

Karastathis, V. K., Karmis, P. N., Drakatos, G., and Stavrakakis, G. (2002). Geophysical methods contributing to the testing of concrete dams. Application at the Marathon Dam. *Journal of Applied Geophysics* v. 50: 247-260.

Keiswetter, D., and Steeples, D. (1994). Practical modifications to improve the sledgehammer source. *Geophysical Research Letters* v. 21: 2203-2206

Keiswetter, D., and Steeples, D. (1995). A field investigation of source parameters for the sledgehammer. *Geophysics* v. 60: 1051-1057.

Lay, T., and Wallace, T.C. (1995). Modern Global Seismicity. New York: Academic Press

Liu, Q. H. (1997). Using GPR and seismic reflection measurements to characterize buried objects: Large scale simulations. *IEEE International Geoscience and Remote Sensing Symposium*: 1147-1149.

McIntosh, J., McDonnell, J. J., and Peters, N. E. (1999). A tracer and hydrometric study of preferential flow in large undisturbed soil cores from the Georgia Piedmont. *Hydrological Processes* v. 13(2): 139-155.

Miller, K. C., Harder, S. H., Adams, D. C., and O'Donnell, T. Jr. (1998). Integrating high-resolution refraction data into near-surface seismic reflection data processing and interpretation. *Geophysics* v. 63: 1339-1347.

Musgrave, A. W. (1967). Seismic Refraction Prospecting. Tulsa: The Society of Exploration Geophysicists.

Pakiser, L. C., and Mabey, D. R. (1954). Mapping shallow horizons with the reflection seismograph. *Science* v. 21: 740.

Parasnis, D. S. (1997). Principles of Applied Geophysics (5th ed.). New York: Chapman and Hill.

Peters, N. E., Freer, J., and Aulenbach, B. T. (2003). Hydrological Dynamics of the Panola Mountain Research Watershed, Georgia. *Ground Water* v. 41(7): 973-988.

Rashed, M. and Nakagawa, K. (2004). High-resolution shallow seismic and ground penetrating radar investigations revealing the evolution of the Uemachi Fault system, Osaka, Japan. *The Island Arc* v. 13: 144-156.

Rees, W.G. (2001). Physical Principles of Remote Sensing. Cambridge: Cambridge UP.

Schwamborn, G. J., Dix, J. K., Bull, J. M., and Rachold, V. (2002). High-resolution seismic and ground penetrating radar – geophysical profiling of a thermokarst lake in the Western Lena Delta, Northern Siberia. *Permafrost and Periglacial Processes* v. 13: 259-269.

Seol, S. J., Kim, J. H., Song, Y., and Chung, S. H. (2001). Finding the strike direction of fractures using GPR. *Geophysical Prospecting* v. 49: 300-308.

Smith, D. G. and Jol, H. M. (1995). Ground penetrating radar: antenna frequencies and maximum probable depths of penetration in Quaternary sediments. *Journal of Applied Geophysics* v. 33 (1): 93-100.

Steeples, D.W. (1998). Shallow seismic reflection section – Introduction. *Geophysics* v. 63: 1210-1212.

Steeples, D. W., and Miller, R. D. (1998). Avoiding pitfalls in shallow seismic reflection surveys. *Geophysics* v. 63: 1213-1224.

Steeples, D. W., Baker, G. S., Schmeissner, C., and Macy, B. K. (1999). *Geophysics* v. 64: 809-814

Stevens, K. M., Lodha, G. S., Holloway, A. L., and Soonawala, N. M. (1995). The application of ground penetrating radar for mapping fractures in plutonic rocks within the Whiteshell Research Area, Pinawa, Manitoba, Canada. *Journal of Applied Geophysics* v. 33 (1): 125-141.

Toshioka, T., Tsuchida, T., and Sasahara, K. (1995). Application of GPR to detecting and mapping cracks in rock slopes. *Journal of Applied Geophysics* v. 33 (1): 119-124.

Touloukian, Y.S. and Ho, C. S. (1981). Physical Properties of Rocks and Minerals. New York: McGraw-Hill Book Company.

Tromp-van Meerveld, I., Peters, N. E., and McDonnell, J. J. (2005). Effect of bedrock permeability on subsurface stormflow and the water balance of a trenched hillslope at the Panola Mountain Research Watershed, Georgia. In review, *Hydrological Processes*

Tsoflias, G. P., Van Gestel, J. P., Stoffa, P. L., Blankenship, D. D., and Sen, M. (2004). Vertical fracture detection by exploiting the polarization properties of ground-penetrating radar signals. *Geophysics* v. 69 : 803-810.

White, A. F., Bullen, T. D., Schultz, M. S., Blum, A. E., Huntington, T. G., and Peters, N. E. (2001). Differential rates of feldspar weathering in granitic regoliths. *Geochimica et Comochimica Acta* v. 65 (5): 847-869.

White, A. F., Blum, A. E., Schultz, M. S., Huntington, T. G., Peters, N. E., and Stonestrom, D. A. (2002). Chemical weathering of the Panola granite: Solute and regolith elemental fluxes and the weathering rate of biotite. The Geochemical Society, Special Publication 7: 37-59.

Wyatt, D. E., Waddel, M. G., and Sexton, G. B. (1996). Geophysics and shallow faults in unconsolidated sediments. *Groundwater* v. 34 (2): 326-336.

Zumbuhl, A. T. (1998). Spatial modeling of soil depth and landscape variability in a small, forested catchment. Thesis, State University of New York.